POLITECNICO DI TORINO

MASTER THESIS IN BIOMEDICAL ENGINEERING

ECG PRE-PROCESSING & AF DETECTION ALGORITHM for ECG-WATCH DEVICE

Author
Giovanni Di Martino

Advisor
Pasero Eros Gian Alessandro
Co-Advisor
Ferretti Jacopo

June 10, 2020

ABSTRACT

This thesis focuses on two main principal topics, regarding respectively the pre-processing performance analysis and the ECG classification process.

The pre-processing performance analysis was achieved with the combined use of two indexes including the SNR percentual increment and the diagnostic distortion measure (DDM) that were used to optimize filters parameters for respectively maximizing denoising effect and minimizing filtering signal distortion.

The ECG classification process includes a new algorithm for AF detection from ultra-short (10 seconds) single lead ECG records. The AF detection algorithm is composed by two successive classification stages. Firstly, HRV signal is extracted from ECG record and it is then decomposed in 5 beats ROI from which a set of HRV features are extracted and used in the first ROI classification stage through MLP NN. Then, the sequence of classified ROI extracted from each ECG record is transformed into a grey levels image where each ROI corresponds to a pixel. A set of features are extracted from grey levels image and are used in the second image classification stage through MLP NN.

AF detection algorithm was validated with 5-fold cross-validation technique and average performances show a sensibility, specificity, and accuracy of 92.62%, 91.44% and 92.21% respectively.

CONTENTS

1 INTRODUCTION

1.1 ELECTROPHYSIOLOGICAL ANALYSIS

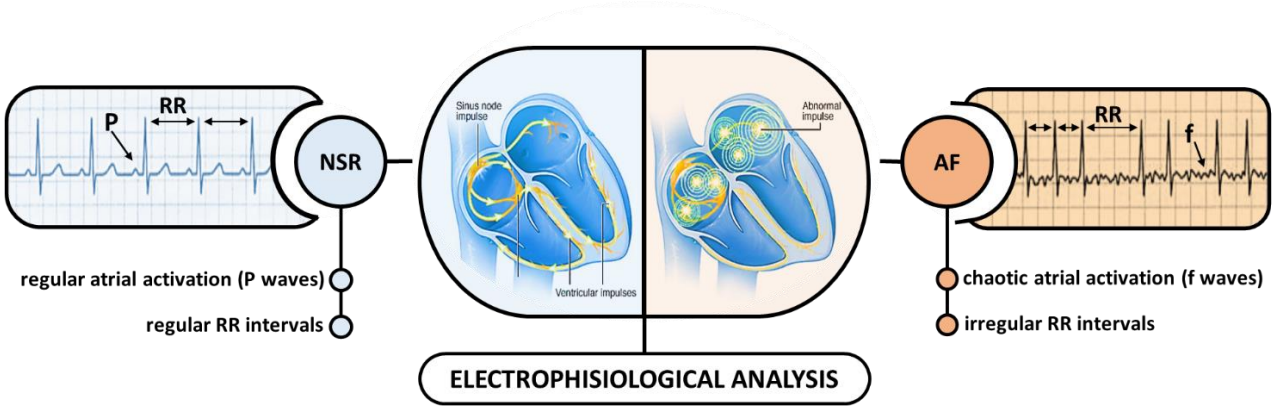

Figure 1

Atrial fibrillation (AF) refers to a disturbance in heart rate that is caused by abnormal electrical activity in the upper chambers of the heart (atria) and no recognizable P waves on electrocardiogram (ECG). During AF episodes, regular action potentials produced by the sinus node for a normal sinus rhythm (NSR) are polluted by rapid electrical impulses produced in the atria. Generally, the two components that favour the establishment of arrhythmia includes slow conduction velocity of cardiac action potential and short refractory period. If the action potential has fast conduction, with a long refractory period, an AF focus would not be established. On the contrary, hearts with shorter duration of action potential and refractory period allow the conduction of re-entrant waves causing non-uniformity of electrical conduction and the insurgent of arrhythmia.

On the surface ECG, AF is described by the irregularity of RR intervals and the presence of irregular and chaotic atrial activation, the fibrillatory f-waves instead of distinct repetitive P-waves. Atrial activity analysis is essential for unquestionable diagnosis of the atrial fibrillation, but a stable, high quality signal without extensive noise is required for the analysis, which is hardly achievable by the ambulatory ECG monitoring. In addition, high heart rate makes it even more difficult to identify atrial activities. Irregular ventricular response, however, is commonly caused by atrial fibrillation, which makes the detection easier. So, an irregular ventricular rhythm may raise suspicion for atrial fibrillation. However, the irregular QRS complexes are just a secondary phenomenon, at the same time there are also other cardiac arrhythmias with irregular heartbeats.

1.2 CLINICAL ANALYSIS

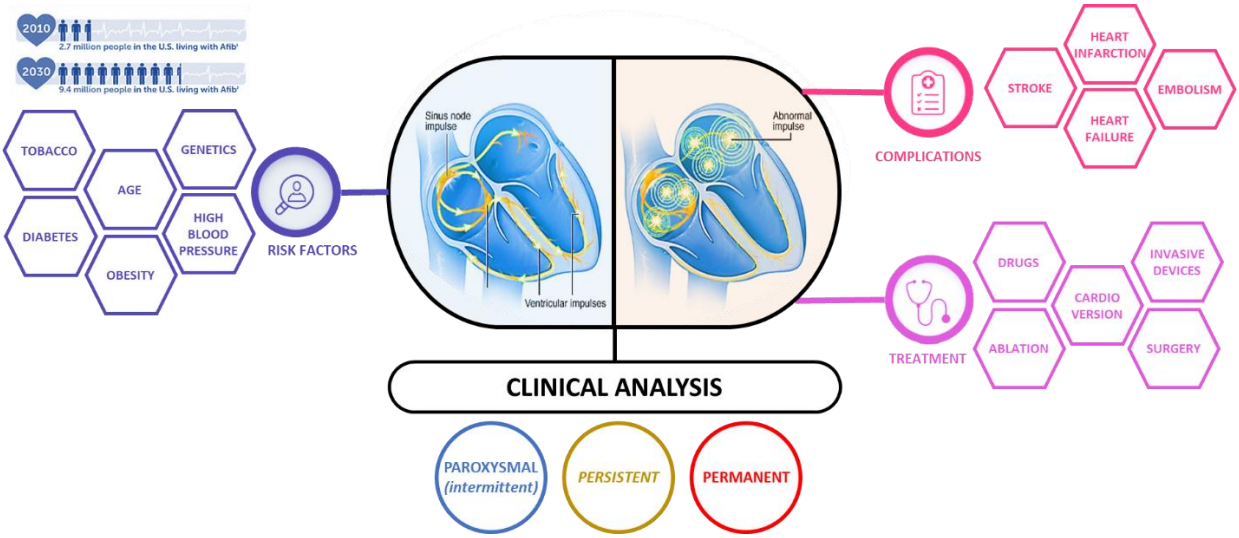

Figure 2

Atrial fibrillation is the most common cardiac arrhythmia worldwide. Its prevalence varies between continents and ethnicity and globally is estimated to be around 30 million. However, AF can be asymptomatic, and it is likely that the estimated prevalence is an underestimate of the true prevalence. Moreover, it is expected to increase significantly in the next 30–50 years due to spreading of risk factors including ageing, high blood pressure, obesity and diabetes. Many other AF risk factors can be identified, and their prevention requires a tailored approach to the individual patient.

AF reduces the efficiency of the heart to move blood into the ventricles, increasing the risk of several complication including heart failure, heart infarction and thrombo-embolic events with consequent strokes.

AF natural evolution usually progresses from short self-terminating rare episodes with little or no symptoms (paroxysmal AF) to longer and more frequent episodes (persistent AF) and finally to permanent AF. An earlier detection of AF could thus allow an earlier adequate management to avoid later complications like circulatory instability, stroke and other ischemic events.

The precise prevalence of patients with asymptomatic or clinically silent AF is by definition unknown, but it has been estimated that among patients with diagnosed AF, one-third does not report symptoms or may experience both symptomatic and asymptomatic episodes of AF. Moreover, the presence or absence of symptoms associated with AF were not associated with differences in the risk of stroke or death. Therefore, detecting patients with paroxysmal AF plays crucial role in earlier protection to developed stage, but data to guide screening are currently unavailable.

When AF is diagnosed, its management is focused on preventing temporary circulatory instability, stroke and other ischemic events. The factors determining AF treatment are duration and evidence of circulatory instability. In order to reduce the risk of systemic-thromboembolism events, oral anticoagulation drugs with the vitamin K antagonists (VKA) can be used. Moreover, rhythm instability can be managed with cardioversion that is indicated with new onset AF episode started within 48 hours. It can be performed with drugs in a chemical way or through the application of a DC electrical shock. If cardioversion is not able to control hear rhythm, it may be necessary to perform electrophysiological studies of abnormal electrical pathways that can be treated is a surgical way with ablation or with cardiac implantable electronic device to control heart rhythm.

1.3 AF DIAGNOSIS PROCESS

Despite its higher prevalence worldwide and its high related risk of stroke, screening for AF is not yet recommended by all scientific AF guidelines, even in specific 'at risk' populations. Early detection of AF at the stage of an asymptomatic arrhythmia, can be discovered incidentally during a routine physical examination, during blood pressure measurement or at a preoperative ECG or cardiology visit.

In general AF is diagnosed at a developed stage when symptoms are evident and the patient go to their general practitioner (GP) with signs and symptoms commonly associated with AF such as feeling dizzy, being short of breath, feeling tired and having heart palpitations.

At the moment, GPs check hear rhythm by taking the patient's pulse by hand. If the GP thinks the patient might have AF, a 12-lead ECG is arranged (*Fig. 3)*. 12-lead ECGs use several pads stuck to the patient's arms, legs and chest to measure how the heart is working. The guidelines for the diagnosis of atrial fibrillation developed by the European Society of Cardiology (ESC) with the special contribution of the European Heart Rhythm Association (EHRA) and endorsed by the European Stroke Organisation (ESO), express that AF diagnosis requires at least 30 s of absolutely irregular RR intervals and no discernible, distinct P waves on electrocardiogram.

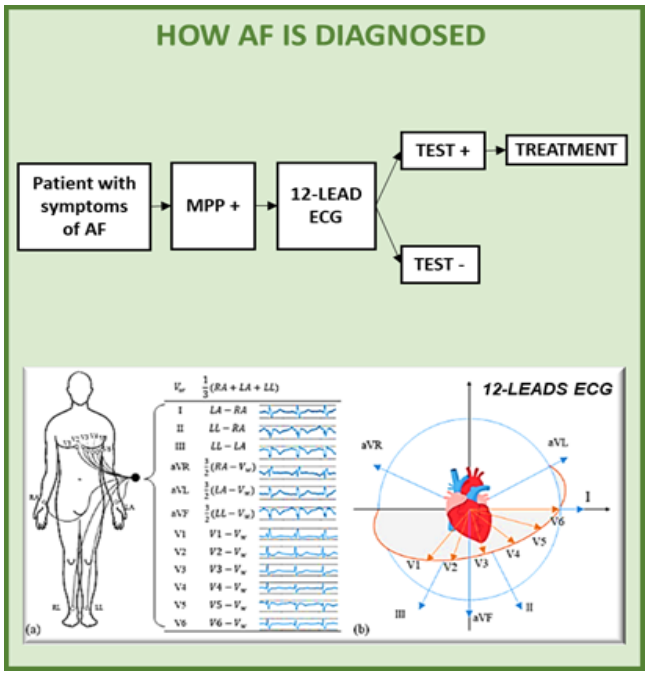

Figure 3

Sometimes a 12-lead ECG can be carried out in the GP practice on the same day as the original appointment. However, it may not be possible to get an appointment on the same day or the GP practice may not have its own 12-lead ECG. If the 12-lead ECG cannot be carried out on the same day, patients may have to travel to be tested and the arrhythmia may have subsided by the time the 12-lead ECG is recorded.

Lead-I ECGs can be a useful tool for testing whether people may have AF (*Fig. 4*). Lead-I ECGs are handheld devices with software to detect AF. By using lead-I ECG devices during GP appointment may mean that AF can be detected earlier than traditional diagnosis practice. Any clinical suspicion of AF, or irregular heart rate evidenced by these devices, should however be confirmed by a 12-lead ECG. However, if AF is detected by using lead-I ECG devices in the GP surgery, high risk people can benefit from anticoagulation to prevent stroke earlier than they currently do because of the asymptomatic nature of AF.

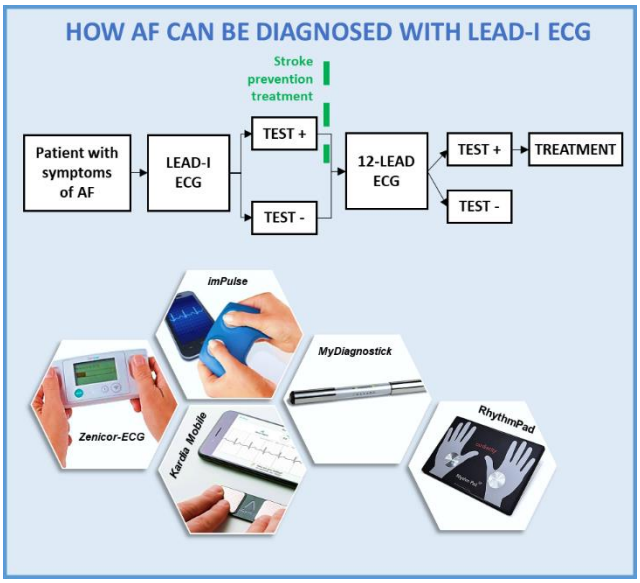

Figure 4

Many non-invasive devices for a simplified lead-I ECG recording are improving, and the key issue becomes whether AF screening can be conducted in a more systematic, comprehensive, and cost-effective manner. Repeated registrations are more effective in catching intermittent episodes compared to single ECG recordings or 24–48 h of long-term ECG. Significant problem with screening studies is the burden of work related to ECG analysis performed with visual control of the tracings. Therefore, automatic algorithms capable to efficiently discriminate normal sinus rhythm from any kind of supraventricular arrhythmias including AF are most welcome.

Given that many patients have associated comorbidities and would seek medical attention, opportunistic screening may be one way of improving detection of AF. Available screening technologies are improving, and the key issue becomes whether AF screening can be conducted in a more systematic, comprehensive, and cost-effective manner. However, given the possible paroxysmal nature of AF, any screening, apart from continuous monitoring, will only give single or occasional snapshots, resulting in possible false negative results. Single led portable devices are an opportunity to improve AF screening capabilities allowing patients to record short ECG signals in any moment so that AF events can be more easily detected with repeated registrations.

1.4PROPOSED SOLUTION

In this context, a new wearable single lead ECG device for medical diagnosis and patient monitoring is being developed in Neuronica Labs of Politecnico of Turin. It is called “ECG Watch” and it is a watch-like recorder equipped with two electrodes positioned on the back and on the top sides of the case. Its design is generally reported in Fig. 5. The case is a 3D-printable plastic case that has been designed in partnership with two students of Department of Architecture and Design (DAD) of Politecnico di Torino.

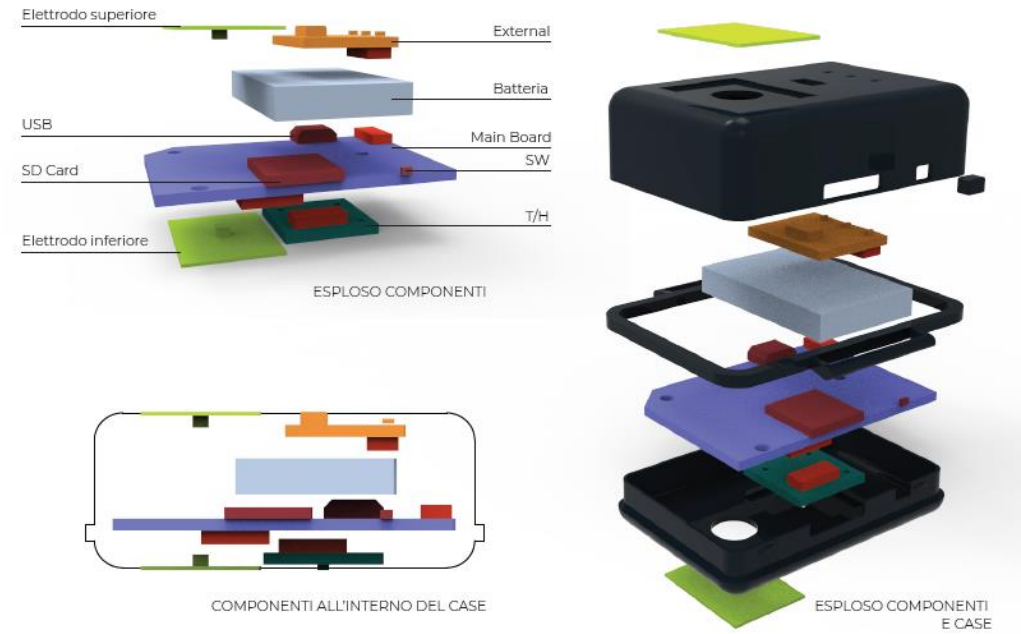

Figure 5

The back electrode is always in contact with the skin. When the patient places opposite harm thumb on the top electrode, 10 seconds lead-I ECG can be recorded and are sent via Bluetooth connection to a mobile app for following elaborations (Fig. 6).

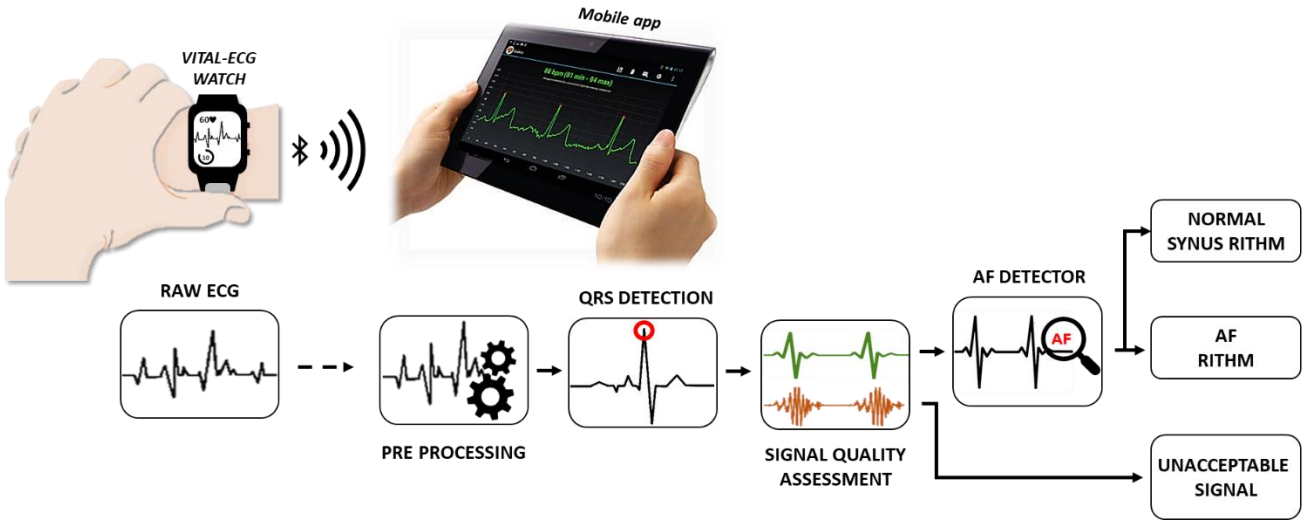

Figure 6

The guidelines for the diagnosis of atrial fibrillation express that AF diagnosis requires at least 30 s of absolutely irregular RR intervals and no discernible P waves on electrocardiogram. The aim of this thesis is to assess the accuracy of AF detection within 10 seconds ECG signals by providing and analysing classification results of very short ECG records.

Firstly, it is important to notice that the recorded ECG signal can be affected by several noise sources and artifacts that can compromise the morphological and diagnostic interpretability of the ECG signal. In particular, these ECG records are mostly contaminated by electrode motion artifacts and muscle noise artifacts caused by the instability of the contact between the front electrode and the thumb. Detailed characteristic about the ECG signal and noises will be provided in chapter 2 and several filtering techniques are discussed in chapter 3. In particular, two filtering parameters have been considered to compare several filtering techniques. The first parameter is the filtering performances expressed as the increment of SNR between noisy and filtered signal. The second parameter is the diagnostic distortion measure (DDM) that measure the distortion between the filtered and clean signal introduced by filters.

When the mobile application receives the ECG record, firstly a pre-processing stage is applied, and it has been built with selected filtering techniques that achieves best performance of SNR increment and lowest distortion.

Then QRS complexes are detected by using two different detector algorithms, that will be detailed in chapter 4. The first is an originally developed wavelet-based algorithm and the second is the well-known Pan-Tompkins algorithm. These two QRS detectors have different performance specially when noisy ECG signals are processed. Thus, by comparing QRS detectors results with each other, a discriminant condition for assessing signal quality can be retrieved when results differ from each other. It is the first important classification stage in which too noisy ECG signal that are not suitable for following elaboration can be detected and classified as unacceptable. Further details of signal quality assessment process will be provided in chapter 5.

If the signal quality is acceptable, a new originally atrial fibrillation (AF) detection process (Fig.7) has been applied. The AF detection algorithm, that is detailed in chapter 6, is based on heart rate variability (HRV) features extracted from RR time intervals exploiting the natural AF characteristic to be “irregularly irregular” heart rhythm that consequently increases both variability and complexity of RR intervals series. The P wave features require very good quality signals to be extracted and analysed due to small P wave amplitudes that can be easily corrupted by noises. Therefore, P wave detection process is currently not considered but will be developed in a future work.

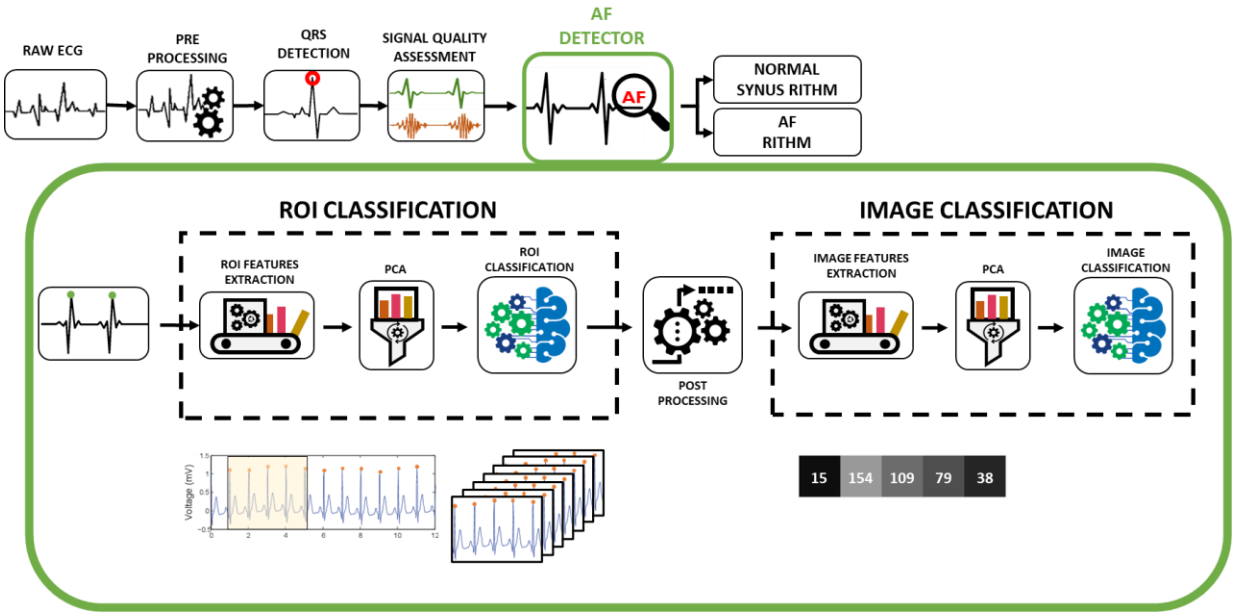

Figure 7

The algorithm is composed by two consecutive classification processes. The first process decomposed the ECG signal into a collection of 5 beats ROI (region of interest) from which several HRV features have been extracted and reduced to improve classification performances. Each ROI was then classified using MLP (multi-layer perceptron) NN which output is a continuous function that has been used as input for the second classification stage. The output of the first classification stage has been transformed into a grey scale image where each pixel corresponds to a ROI of the original ECG signal. Several density and probability distributions features have extracted from the image and was finally classified using a second MLP NN into AF class or NSR class.

2 ECG & NOISE

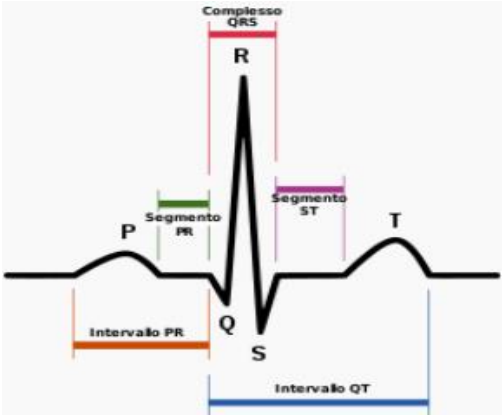

Figure 8

The electrocardiogram (ECG) shows the electrical activity of the heart, where each heartbeat is displayed as a series of electrical waves (Fig.8). ECG signal is characterized by five peaks and valleys labelled by the letters P, Q, R, S, T that express heart functions information. Mainly an ECG tracing is a repeating cycle of three electrical entities: P wave (atrial depolarization), QRS complex (ventricular depolarization) and a T wave (ventricular repolarization). Normally, the frequency range of an ECG signal is of 0.05–50 Hz in which the P wave lies in 0.67 to 5 Hz, QRS complex in 10 – 50 Hz and T-wave in 1 to 7 Hz.

ECG signal is affected by different noises during its acquisition and transmission. Several noise sources can corrupt the ECG signal and they can be generally grouped basing on their power spectral density (PSD) (Fig. 9). Noises with high frequency include electromyogram (EMG) noise, additive white Gaussian noise, and power line interference which their principal power spectral density in localized on higher frequencies than ECG signal frequency range. Noises with low frequency include baseline wandering that affect the ECG signal in lower frequency range. Moreover, several artifacts can corrupt ECG including electrodes motion artifacts and muscle artifacts which PSD mostly overlap ECG signal bandwidth and therefore are the most difficult to remove.

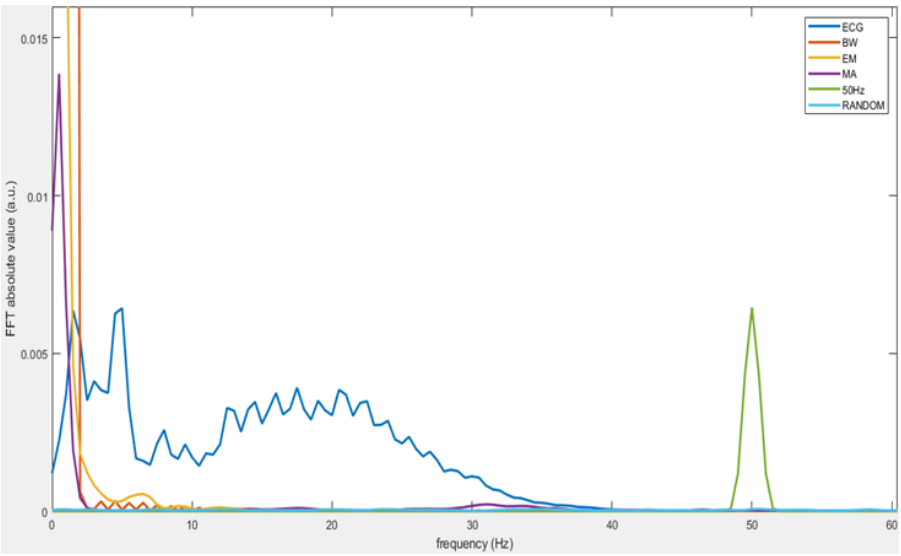

Figure 9

2.1 NOISES ANALYSIS

Baseline Wander:

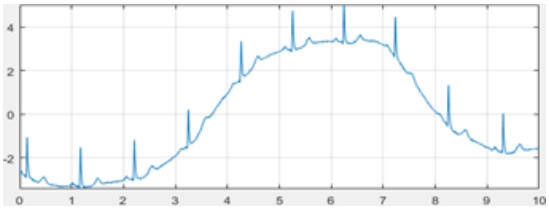

Figure 10

Baseline wander or baseline drift is the effect where the base axis (x-axis) of a signal appears to 'wander' or move up and down rather than be straight. This causes the entire signal to shift from its normal base that normally is a zero-mean signal. The baseline wander is caused due to improper electrodes (electrode-skin impedance), patient's movement and breathing (respiration). The frequency content of the baseline wander is in the range of 0.5 Hz. However, increased movement of the body during exercise or stress test increase its frequency content.

Power line interference:

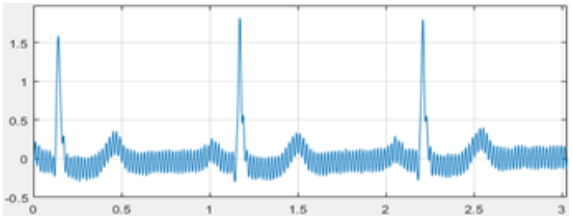

Figure 11

Electromagnetic fields caused by a powerline represent a common noise source in the ECG, as well as to any other bioelectrical signal recorded from the body surface. Such noise is characterized by 50 (or 60 Hz) sinusoidal interference, possibly accompanied by several harmonics. Such narrowband noise renders the analysis and interpretation of the ECG more difficult since the delineation of low-amplitude waveforms becomes unreliable and spurious waveforms may be introduced. The interference is mainly caused by electromagnetic field (EMF) interference generated by the alternating current fields in power line or nearby machines.

Electromyogram (EMG) Noise

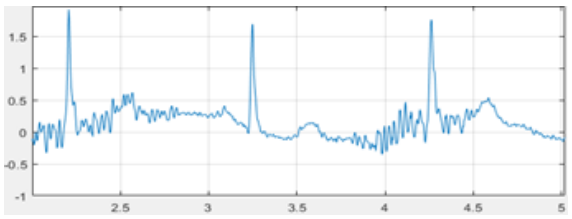

Figure 12

The presence of muscle noise represents a major problem in many ECG applications, especially in recordings acquired during exercise, since lower amplitude ECG waveforms may become completely obscured. Muscle noise is not removed by narrowband filtering, but presents a much more difficult filtering problem since the spectral content of muscle activity considerably overlaps that of the PQRST complex.

Electrode Motion Artifacts

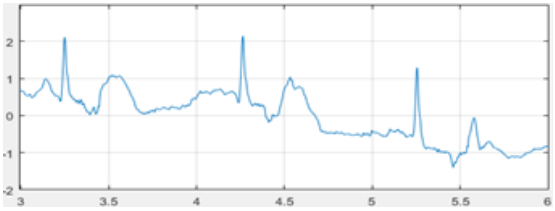

Figure 13

Electrode motion artifacts are mainly caused by skin stretching which alters the impedance of the skin around the electrode. Motion artifacts resemble the signal characteristics of baseline wander but are more problematic to combat since their spectral content considerably overlaps that of the PQRST complex. They occur mainly in the range from 1 to 10 Hz. In the ECG, these artifacts are manifested as large-amplitude waveforms which are sometimes mistaken for QRS complexes. Electrode motion artifacts are particularly troublesome in the context of ambulatory ECG monitoring where they constitute the main source of falsely detected heartbeats.

3 PRE-PROCESSING

Noise sources contaminating in the ECG signal may lead to wrong diagnostic interpretation and therefore it is necessary to remove them. Pre-processing aim focuses on attenuating noises and artifacts components while preserving PQRST morphological characteristics that are important in diagnostic interpretation of the signal.

In this section, several signal processing methods have been investigated and their performance compared. Moreover, filtering noise performances have been evaluated considering one single noise source at a time (Fig. 14). The aim is to select best filters and combine them to create a noise reduction process. Generally, a denoising process consists of a low pass filter to remove high frequency noises including random noise, a high pass filter to remove base line drifts including base wander noise and a notch filter to remove 50 Hz power line interference. Therefore, the investigation has been mainly focused on tuning the design of proposed filter to find optimal design configuration for each noise source. Filtering performances have been evaluated using two quantitative indexes that will be discussed later that quantify SNR increment and the morphological distortion induced by filters. Great attention has been focused on choosing most suitable filters that are good in preserving diagnostic morphological information of ECG signal.

The proposed denoising techniques can be generally grouped into three filters types:

- Moving window filters including moving average filters, moving median filters, and moving regression filters are often used for noise reduction but their performances are highly sensitive to the selection of window length.
- Finite impulse response (FIR) filters are broadly used because of their stability but they can introduce considerable distortion in the ECG signal.
- Wavelet filters are very efficient, but the selection of appropriate wavelet function and threshold plays an important role in signal denoising.

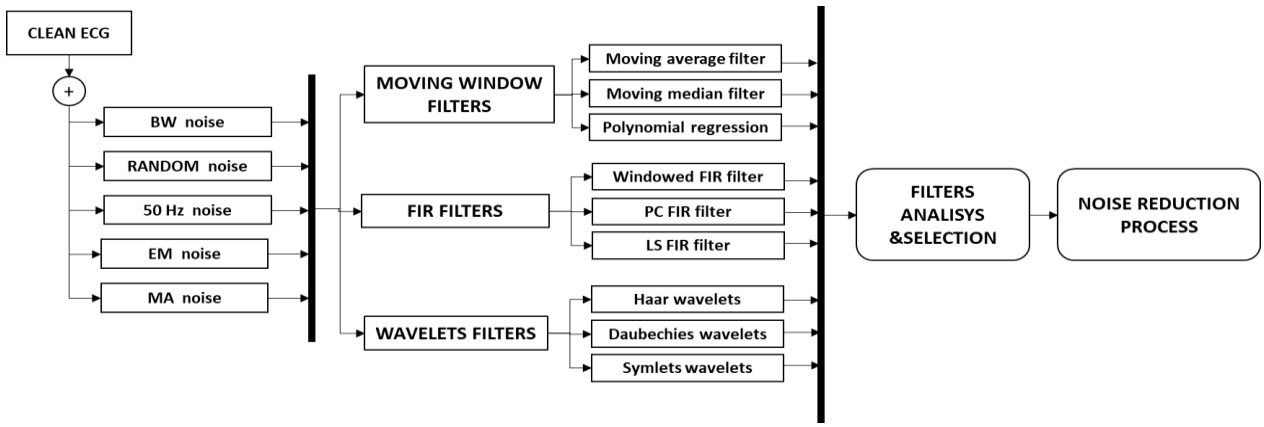

Figure 14

3.1MOVING WINDOW FILTERS

Moving Average Filter

The moving average filter smooths data by replacing each data with the average of its neighbouring data defined within the span. This process is equivalent to lowpass filtering with the smoothing response given by the following form:

$$y_n = \frac{1}{M} \sum_{i=-\frac{1}{2}(M-1)}^{\frac{1}{2}(M-1)} x_{n-i}$$

where x_n denotes a noisy ECG signal, y_n is the smoothed signal and M is the length of the moving window.

By subtracting the output y of this filter from original signal x, the data equivalent to high pass filtering.

The high or low cut-off frequency (fc) is determined by the window length

$$f_c = \frac{f_s}{2M}$$

Moving average filtering is a simple method for both low and high frequency noise reduction. However, since the QRS complex of the ECG signal has an extreme amplitude that affects the average, this method introduces signal distortions depending by the choice of filter length M.

Moving Median Filter

The moving median filter is based on same principles as the moving average filter, in which the median within a moving window of a given length is calculated instead of the average.

Median operator has different properties respect the average operation especially when working with outliers. The non-linear nature of median filter allows it to be less sensitive to outliers than average filter. This is important when referred to abrupt spikes, like QRS complexes, where extreme amplitude values can be considered as outliers.

Generally, moving window filters work well with spikes shorter than window length while preserving larger spikes. Thus, it is recommended to use a window length shorter than QRS complex length in order to preserve QRS morphology.

Polynomial Regression Filter

Polynomial local regression method, initially developed for scatterplot smoothing, is a LOESS method (locally estimated scatterplot smoothing) that combines much of

the simplicity of linear least squares regression with the flexibility of nonlinear regression.

It can be used as non-parametric denoising technique by fitting simple polynomial model to a localized subset of ECG signal windowed using a sliding window. By using higher-order polynomials the likelihood of producing an accurate smoothed signal increases, although it is obviously linked to an increased computational complexity. LOESS method with a 2nd degree polynomial model has been chosen for following evaluations.

3.2 FIR FILTER

Finite impulse response (FIR) filters are characterized by finite duration impulse response, in contrasts with infinite impulse response (IIR) filters, which may have internal feedback and may continue to respond indefinitely (usually decaying). The impulse response of an Nth-order discrete-time FIR filter lasts exactly N + 1 samples (from first nonzero element through last nonzero element) before it then settles to zero.

For a discrete-time FIR filter of order N, each value of the output signal is computed by a weighted sum of the most recent input values as described by the following equation that perform a discrete time convolution operation:

$$y(n) = \sum_{m=0}^{N-1} b_m x(n-m)$$

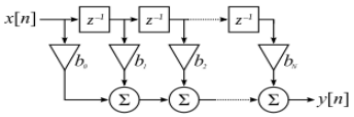

where b_m are the coefficients of the filter, N - 1 is the order of the filter, N is the length of the filter, x(n) is the input signal, y(n) is the filtered signal.

Generally, FIR filters have some properties which sometimes make them preferable to infinite impulse response (IIR) filters. Firstly, FIR filters do not require feedback loop so that rounding errors are not compounded by summed iterations and the same relative error occurs in each calculation. Secondly, they are inherently stable since they can be easily designed to be linear phase by making the coefficient sequence symmetric. This property is desired for reducing signal distortion because of non-linear phase response. The main disadvantage of FIR filters is that are considerably more computation power compared to an IIR filter with similar design filter requirements.

FIR filters are designed by finding the coefficients and filter order that meet certain specifications settled by the user. In this study, three different design methods have been discussed: Window design method, least squares design and Parks-McClellan method.

WINDOWED FIR FILTERS

The window design method truncates an IIR filter by multiplying it with a finite length window function. Multiplying the infinite impulse by the window function in the time domain results in the frequency response of the IIR being convolved with the Fourier transform of the window function. The result the frequency domain convolution is FIR filter whose frequency response is modified from that of the IIR filter because the edges of the rectangle are tapered, and ripples appear in the passband and stopband. Working backward, filter specification can be initially settled by specifying the slope (or width) of the tapered region (transition band) and the height of the ripples, and thereby derive the frequency domain parameters of an appropriate window function.

LEAST SQUARE FIR FILTERS

The weighted least squares design uses an error criterion that is based on the energy of the signal and the design equations are linear. However, the designs sometimes have frequency response with oscillations or overshoots that may be undesirable. Since the energy of the signal is related to the square of the signal, a squared error approximation criterion is often appropriate.

PARKS-McCLELLAN FIR FILTERS

The Parks–McClellan algorithm, is an iterative algorithm for finding the optimal Chebyshev finite impulse response (FIR) filter. It is utilized to design and implement efficient and optimal FIR filters by calculating optimal filter coefficients through an indirect method. The goal of the algorithm is to minimize the error in the pass and stop bands by utilizing the Chebyshev approximation. The Parks–McClellan algorithm is a variation of the Remez exchange algorithm, with the change that it is specifically designed for FIR filters. It has become a standard method for FIR filter design.

3.3WAVELETS FILTERS

Wavelet filters are created by a “mother” wavelet and a scaling function associated to that wavelet. The wavelet function satisfies the admissibility conditions for zero mean and for square norm one, that imply wavelet is a finite energy function.

The discrete wavelet transforms (DWT) of the signal x(t) is defined as follow:

$$DWT_x(b,a) = \frac{1}{\sqrt{a}} \int_{-\infty}^{+\infty} x(t) g^* \left(\frac{t-b}{a}\right) dt$$

where g(x) is the wavelet function, and b and a are the translation and dilation parameters, respectively. The duration of the mother wavelet g(t) is either compressed or expanded depending upon the choice of a. In discrete wavelet

transform, the scaling function is discretized and is expressed on a dyadic scale $2^j$where (j=1, 2…, n) represent each scale. With smaller scales, the support for the wavelet decreases and the wavelet transform becomes more sensitive to high-frequency components of the signal. On the contrary, lower frequency components of the signal are reflected with larger scales.

The DWT can also be considered as the output of a bank of bandpass filters whose centre frequencies and bandwidths vary depending on the dilation parameter a in addition to the spectral properties of the wavelet function. The variable bandwidth introduces different resolutions at different scales and thus, the DWT has a multiresolution capability.

The discrete wavelet multi-resolution analysis allows to compute wavelet filters coefficients at every possible scale. The original signal frequency spectrum is iteratively decomposed into high and low frequency signals by using series of conjugate mirror filter pairs that usually denote the filter banks at reconstruction.

The signal is iteratively projected onto a multi-resolution approximation space that is decomposed into a lower resolution (approximation) space representing lower frequency components obtained by the low pass filter, and a detail space representing higher frequency components obtained by the symmetric high pass filter. The orthogonal basis in the lower resolution space is then divided into two new orthogonal bases at each iteration step (Fig. 15). At decomposition, the wavelet coefficients are generated by low pass and high pass filters and they are called approximates and detail coefficients respectively.

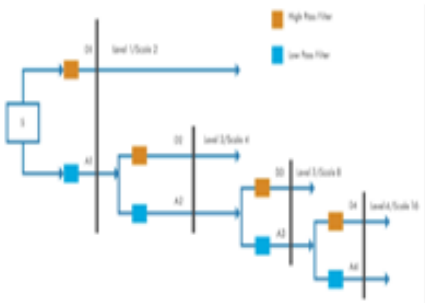

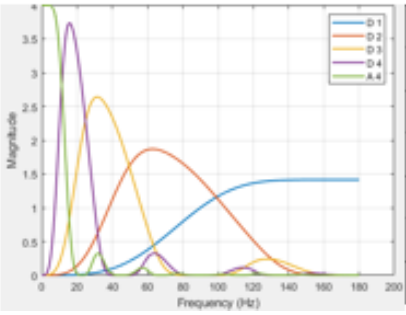

scale	Bandwidth (Hz)
$s = 2^1$	90-180 Hz
$s = 2^2$	45-90 Hz
$s = 2^3$	22,5 – 45 Hz
$s = 2^4$	11,25 – 22,5 Hz
$s = 2^5$	5,62 – 11,25 Hz
$s = 2^6$	2, 81 – 5,62 Hz

Figure 15

Therefore, signal bandwidth is iteratively divided in the approximation and detailed space for each scale analysed.

It is important to identify which mother wavelet is best suited for the detection of given pattern. Several wavelet functions have been considered in this study and their performances compared. The analysed wavelets belong to different wat family types: the Daubechies wavelets and the Symlets wavelets (Fig.16).

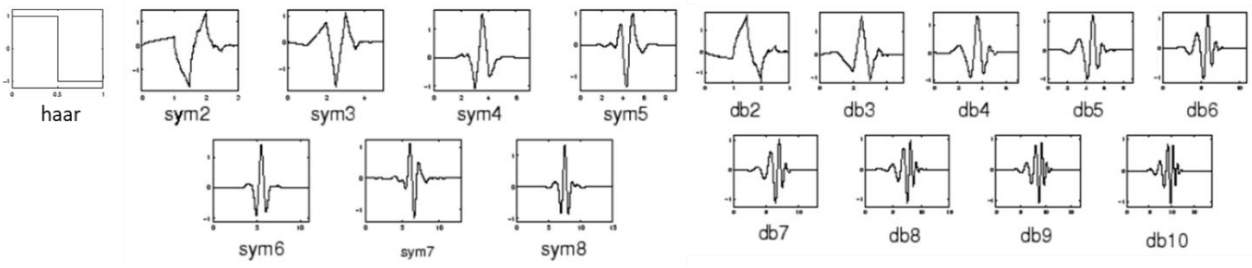

Figure 16

3.4 PERFORMANCE EVALUATION METHOD

3.4.1 SYNTHETIZED NOISY SIGNALS

To evaluate and compare noise reduction performance of different signal-processing techniques, synthetic noisy ECG signals were constructed by adding thoughtful amount of different types of noise to a clean ECG. The experimental signals were synthesized from 10 seconds clean ECG recording by adding 10 seconds of different noisy sources including electrode motion artifacts, muscle artifacts, baseline wander noise, power line (50 Hz) interference noise and random white gaussian noise (Fig.17). Noises records (from Physionet Database) are weighted by a gain factor in order to add a calibrated amount of noise to obtain specific SNR ratio for each synthesized noisy signal. The gain factor is computed with the Newton method that iteratively find the optimal gain factor to obtain the closest SNR ratio to the desired one.

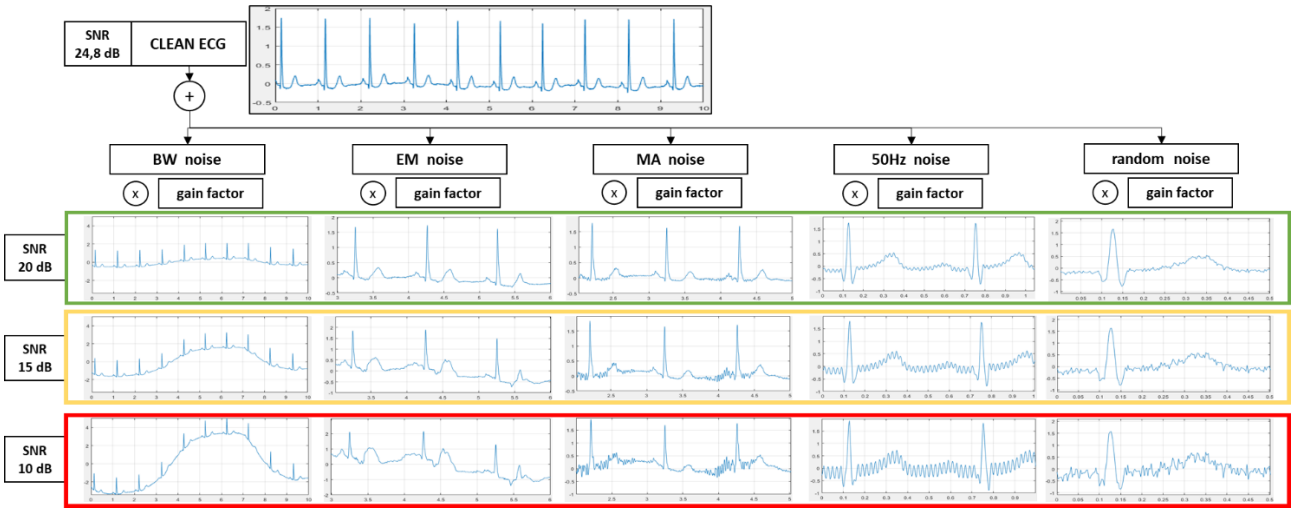

Figure 17

In order to evaluate noise reduction performance, various method can be used. These methods can be divided into two main groups: subjective methods and objective methods. Subjective methods are based on the assessment of ECG signal quality by cardiologists or other experts while objective methods are based on mathematical equations, and hence there is no need for expert human assessment. The subjective methods for ECG quality evaluation are medically accepted, and they

can be used to qualitatively assess filtering performances. Objective methods were used to quantitatively evaluate the performance of different denoising methods. In this study, two parameters where chosen for quantitative analysis: SNR index ratio that quantify the ratio of signal power to noise power, and the diagnostic distortion measures (DDM) that quantifies the distortion percentage of the filtered signal from the original one focusing on diagnostic characteristics of PQRST complexes. Both parameters for noise reduction performance analysis need ECG signal to be characterized by localizing peaks and valley of principal ECG waves.

3.4.2 ECG CHARACTERIZATION

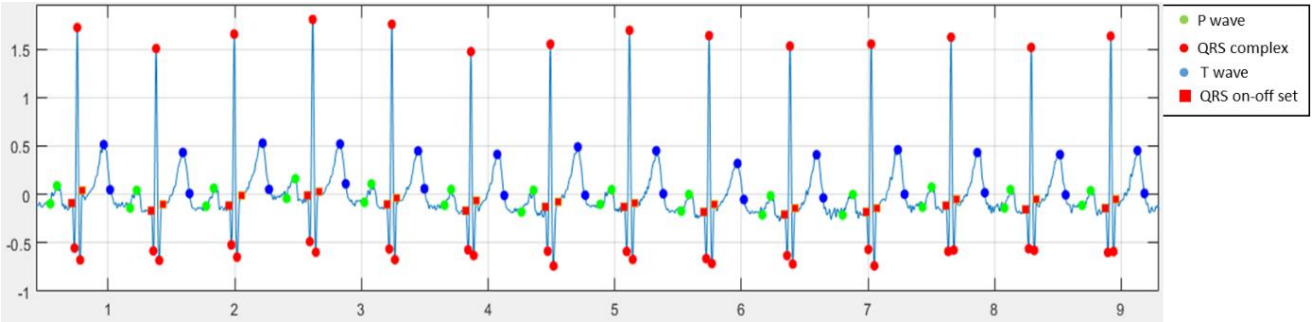

Figure 18

The first step for every ECG signal analysis is the characterization of peak and valley by localizing PQRST waves of each heartbeat (Fig.18). The characterization starts from R peaks detection algorithm results that provides R waves time localization. R peak waves are the first and easiest waves to be localized due to their extremely high amplitude from all other ECG waves. In this study two automatic R peak detectors have been developed and they will be detailed in the next chapter.

Starting from R peaks positions each heartbeat can be windowed and characterized by localizing following points:

- QRS complex points including the on-set and the off-set points that define QRS complex width.
- P wave including the onset P wave point that defines the start of heartbeat window.
- T wave including the off-set T wave point that define the end of heartbeat window.

3.4.3 SNR INDEX

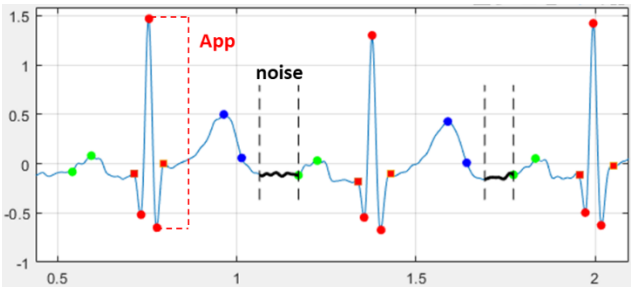

Figure 19

Signal to noise ratio (SNR) is a commonly used index to measure the relative signal power from noise power corrupting the signal. In ECG signal application, noise power can be computed on the isoelectric period between two consecutive heartbeat where no heart electrical activity exists and only noise is present (Fig.19). By assuming noise is a standard gaussian distribution, noise power can be computed as the standard deviation of the isoelectric period. Signal power is computed as squared peak-to-peak signal amplitude.

$$SNR = 20\ log_{10}\left(\frac{A_{pp}}{4 * std(noise)}\right)$$

In this study, the normalized SNR difference (ΔSNR) between the noisy synthesized ECG signal and the filtered one has been considered. The normalized SNR difference corresponds to the percentage variation of SNR that is positive if filtered SNR index increase, while is negative if SNR index decrease.

3.4.4 DIAGNOSTIC DISTORTION MEASURE

The diagnostic distortion measure is computed as linear combination of normalized difference of several morphological features between the clean ECG signal and filtered one.

Starting from the characterization of the ECG record, several amplitude and time features are extracted from each single windowed beat (Fig. 20). These features are:

- 4 AMPLITUDE FEATURES including the peak-to-peak amplitude between RS, QR, RT waves and the ST segment elevation from the S amplitude depolarization level.
- 4 TIME INTERVAL FEATURES including QRS complex interval, PQ, ST, QT interval.
- 2 AREA FEATURES including PQ interval area under curve and ST interval area under curve.

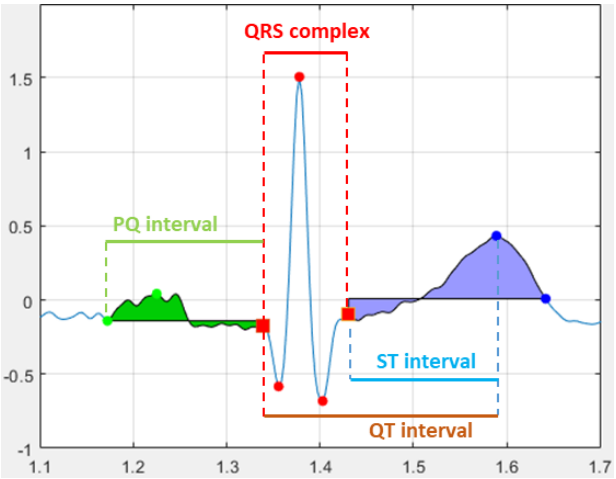

Figure 20

For each windowed beat, a vector of features β and $\beta^{\bullet}$ is extracted by the original clean ECG windowed signal and the filtered one, respectively. For each beat the diagnostic distortion measure (DDM_{beat}) is computed as linear combination normalized difference of the n morphological features:

$$DDM_{beat} = \sum_{i=1}^{n} \left| \frac{\beta - \beta^{\bullet}}{\beta} \right| \; x\ 100$$

The total distortion measure (DDM_{tot})between the original ECG and the filtered signal is computed as the average value of each beat distortion measure:

$$DDM_{tot} = \frac{1}{M} \sum_{i=1}^{M} DDM_i$$

Where M is the number of beats in ECG signal.

3.5 FILTERING PERFOMANCE ANALYSIS

The aim of this section is to analyse several filtering performances technique among those previously described and select the most suitable filter techniques to create optimal noise reduction process. Generally, noise reduction process is composed by the combination of low pass, high pass and power line interference filters. Filtering performances are evaluated considering synthetized noisy signals where one noise source is considered individually. In particular to investigate low pass, high pass and notch filters performances, a clear ECG signal is respectively corrupted by base wander noise, random white gaussian noise and power line noise.

Each filter belonging to filter families under investigation have been tested and their designs have been optimized tuning their parameters. Denoising performances have been evaluated using the diagnostic distortion measure (DDM) and SNR variation percentage (ΔSNR). For each noise source the optimal design that maximise ΔSNR and minimize DDM is selected. By comparing the optimal filter design of each filter family, the best filter technique is selected for each noise source including base wander noise, random white gaussian noise and power line interference.

Finally, by combining the selected low, high and notch filters, a noise reduction process has been assembled. The assembled noise reduction process has been tested and validated on ECG signal corrupted with muscle and electrode motion artifacts which power spectral density (PSD) mostly overlap ECG bandwidth.

3.5.1 BASE WANDER NOISE REDUCTION

For each filter family, high pass filters have been tuned to optimize their designs in order to maximise SNR percentage variation (ΔSNR) and minimize diagnostic distortion measure (DDM). Filters have been tested using corrupted ECG signal with different amount of BW noise so that the resulting SNR index was settled to be 20 dB, 15dB, 10 dB (Fig.21)

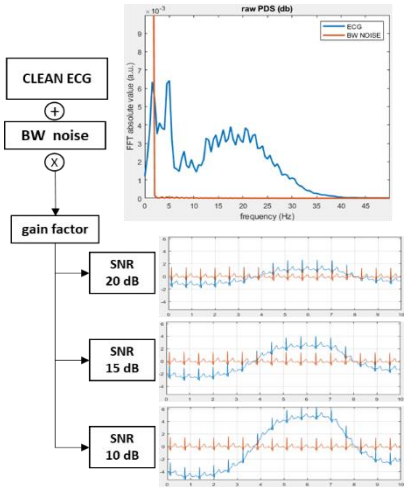

Figure 21

In order to reduce low frequency noises, the 1990 American Heart Association (AHA) document recommended that “the low-frequency cut-off be 0.05 Hz for routine filters but that this requirement could be relaxed to 0.67 Hz or below for linear digital filters with zero phase distortion”. In this recommendation, the requirement of linear digital filters with zero phase distortion is critical because if digital filters have non-linear phase response, phase distortion is introduced into the signal, resulting in distortion of the low-frequency components of the ECG signal.

Both FIR and wavelet filters under analysis have linear phase response and are always stable, so their cut off frequency can be settled to 0,5 Hz.

For each family filter, including moving window filters, FIR filter and wavelets filter, filter design optimization and performance are evaluated for each SNR noisy signal (Fig. 22, 23, 24). For each family type, the best performance filter corresponding to higher SNR difference and lower DDM is highlighted and selected.

Considering moving window filters family (Fig.22), several window lengths between 1 and 2 seconds have been tested for moving average filter, moving median filter and polynomial regression filter. Best performance occurs by using polynomial regression filter with window length 1,5 seconds.

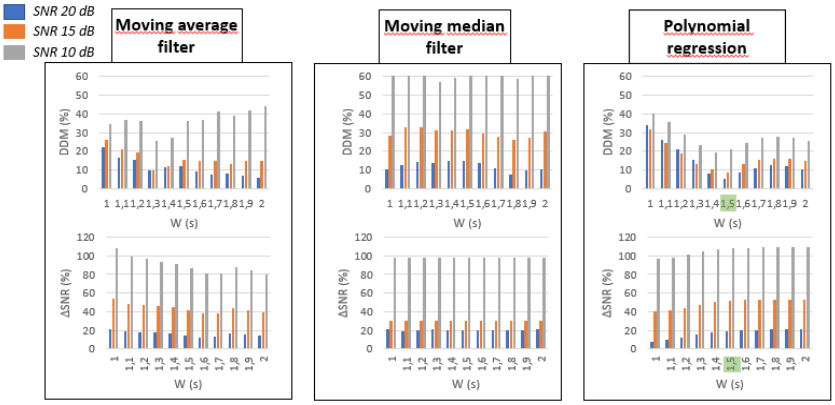

Figure 22

Considering FIR filters types (Fig.23), several orders between 400 and 2000 have been tested for windowed FIR filters, Parks-McClellan filter, and least square filter. Analysing and comparing their performance, best filter performance occurs using least square filter with order 500.

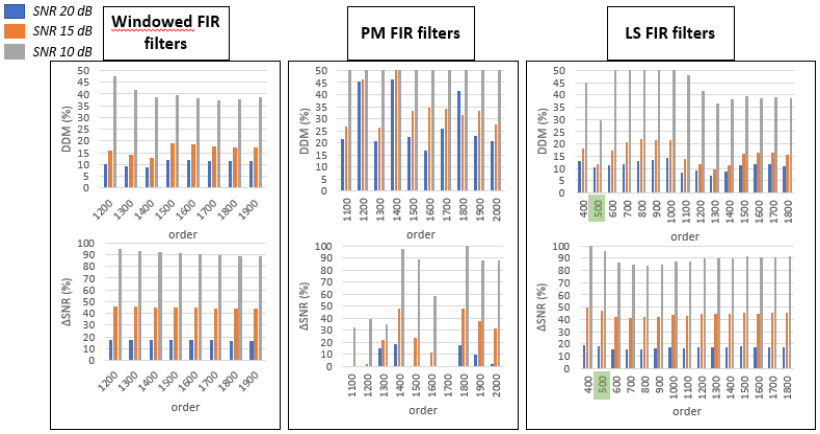

Figure 23

Considering wavelets filters (Fig.24), only scale between 1 and 8 were considered, corresponding to a high pass filter with cut-off frequency of 0.7 Hz. Several wavelets have been tested including haar wavelet, Daubechies wavelets and the Symlets wavelets. Best performance occurs with sym8 wavelet.

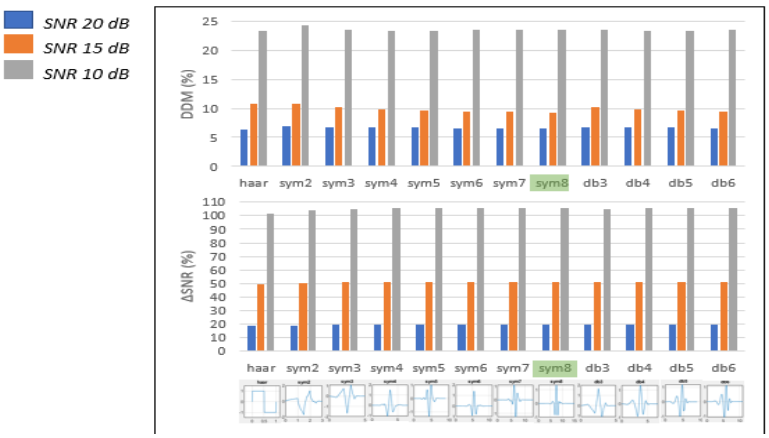

Figure 24

Finally, considering best performance filters previously selected for each family filter, their comparison is evaluated for all SNR noisy signals (Fig. 25). It is evident that best performance that maximise SNR variation (ΔSNR) and minimize distortion measure (DDM) is achieved with polynomial regression filter with window length of 1,5 seconds.

This selected high pass filter will be used to build a noise reduction process in combination with high and notch filters that are going to be selected in next pages.

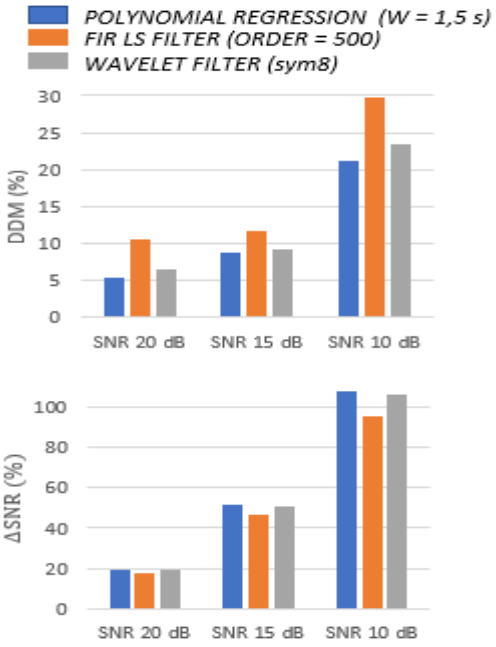

Figure 25

3.5.2 RANDOM WHITE GAUSSIAN NOISE REDUCTION

For each filter family, low pass filters have been tuned to optimize their designs in order to maximise SNR percentage variation (ΔSNR) and minimize diagnostic distortion measure (DDM). Filters have been tested using corrupted ECG signal with different amount of RANDOM white Gaussian noise so that the resulting SNR index was settled to be 20 dB, 15dB, 10 dB (Fig. 27).

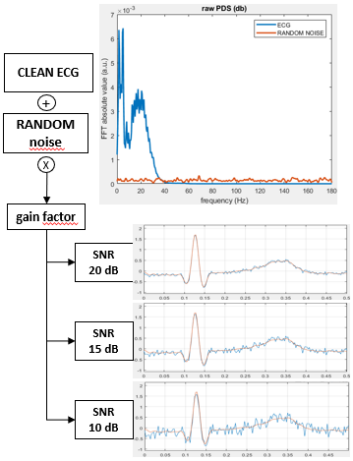

Figure 27

In order to reduce high frequency noise, several low pass FIR filters with cut-off frequency of 45 Hz have been analysed. Moreover, moving window filters have been tested focusing on their smoothing ability.

For each family filter, including moving window filters, FIR filter and wavelets filter, filter design optimization and performance are evaluated for each SNR noisy signal (Fig. 26, 27, 28). For each family type, the best performance filter corresponding to higher SNR difference and lower DDM is highlighted and selected.

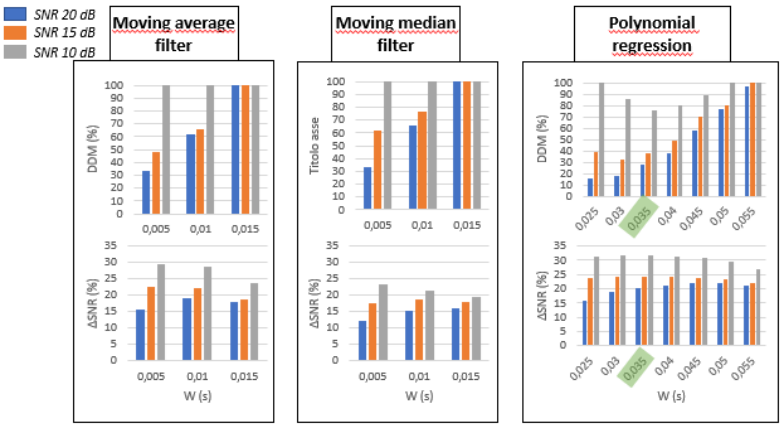

Figure 26

Considering moving window filters family (Fig.26), several window lengths between 0,005 and 0,07 seconds have been tested for moving average filter, moving median filter and polynomial regression filter. Their corresponding cut-off frequency depends upon the choice of window length (M) and is computed as $\frac{1}{2M}$; therefore, the corresponding cut-off frequencies tested vary between 100 Hz and 7,15 Hz. Best performance occurs by using polynomial regression filter with window length 0,035 seconds that is equivalent to 14,3 cut-off frequency.

Analysing FIR filter family, (Fig.27), several orders between 10 and 100 have been tested for windowed FIR filters, Parks-McClellan filter, and least square filter. Analysing and comparing their performance, best filter performance occurs using windowed FIR filter with order 30.

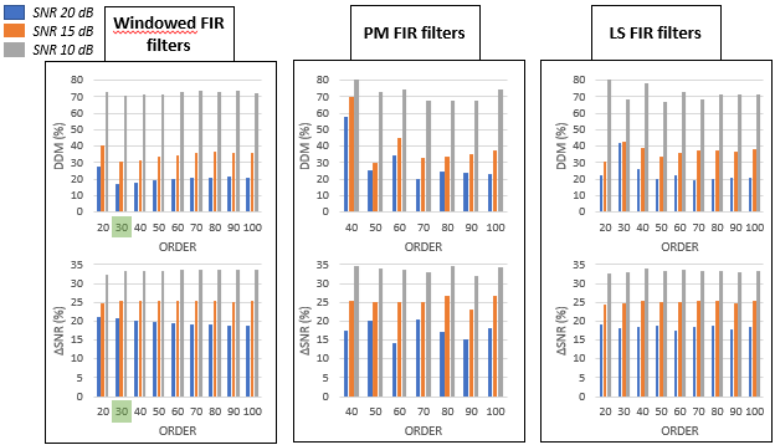

Figure 28

Considering wavelets filters (Fig.28), only scale between 3 and 9 were considered, corresponding to a low pass filter with cut-off frequency of 45 Hz. Several wavelets have been tested including haar wavelet, Daubechies wavelets and the Symlets wavelets. Best performance occurs with sym8 wavelet

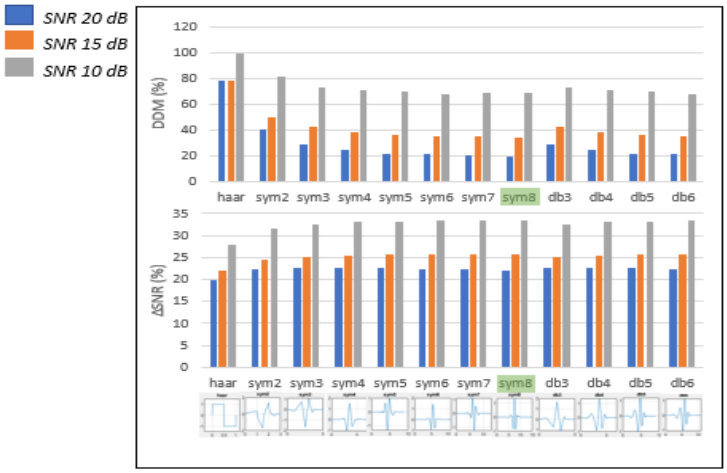

Figure 29

Finally, considering best performance filters previously selected for each family filter, their comparison is evaluated for all SNR noisy signals (Fig. 30). It is evident that best performance that maximise SNR variation (ΔSNR) and minimize distortion measure (DDM) is achieved using windowed FIR filter with order 30.

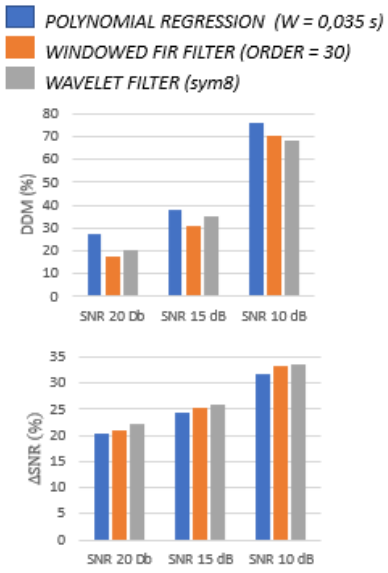

Figure 30

This selected low pass filter will be used to build a noise reduction process in combination with low pass filter previously selected and notch filter that is going to be selected in next pages.

3.5.3 POWER LINE INTERFERENCE REDUCTION

For each filter family, 50 Hz notch FIR filters have been tuned to optimize their designs in order to maximise SNR percentage variation (ΔSNR) and minimize diagnostic distortion measure (DDM). Filters have been tested using corrupted ECG signal with different amount of 50 Hz noise so that the resulting SNR index was settled to be 20 dB, 15dB, 10 dB (Fig. 31).

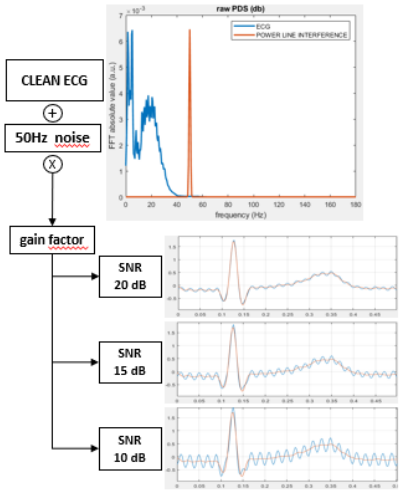

Figure 31

In order to reduce power line interference, several notch FIR filters with cut-off frequency of 50 Hz have been analysed.

FIR filter design optimization and performance are evaluated for each SNR noisy signal (Fig. 32). several orders between 10 and 140 have been tested for windowed FIR filters, Parks-McClellan filter, and least square filter. The best performance filter corresponding to higher SNR difference and lower DDM is highlighted and selected occurs using Parks McClellan FIR filter with order 50.

This selected notch filter will be used to build a noise reduction process in combination with low pass filter and high pass filter previously selected.

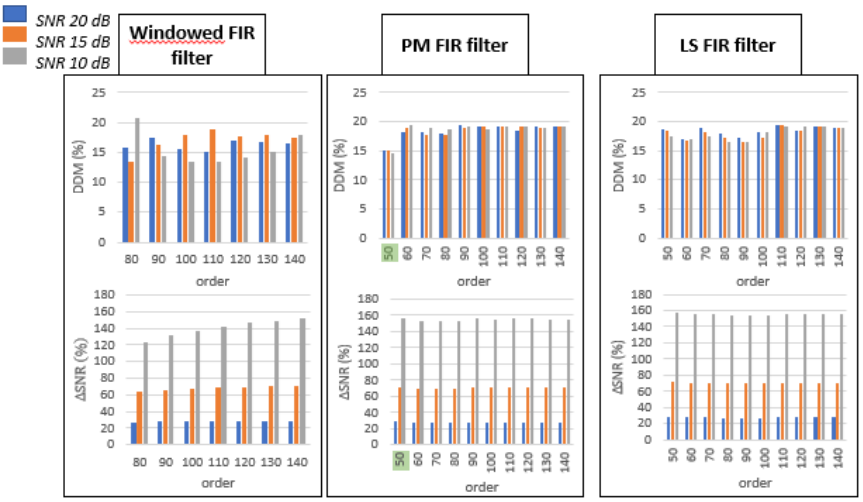

Figure 32

3.6 NOISE REDUCTION PROCESS

Considering the three noise sources previously analysed, the filter that achieved best results have been selected and used to build the noise reduction process (Fig. 33).

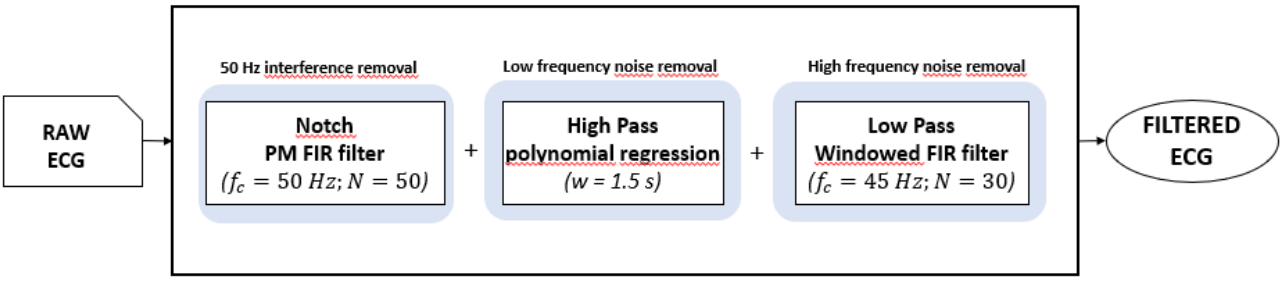

Figure 33

3.6.1 VALIDATION

In order to evaluate noise reduction process performances, it has been validated by filtering noisy synthetized ECG signal corrupted with thoughtful amount of muscle artifacts and electrode noise artifacts individually. These noise sources are different from previously analysed noises because these noises power spectral density mostly overall ECG bandwidth and therefore is much more difficult to obtain good filtering performance using traditional denoising process.

However, considering filtering performance results of these artifacts (Fig. 34), acceptable results were achieved specially when referred to muscle artifacts results.

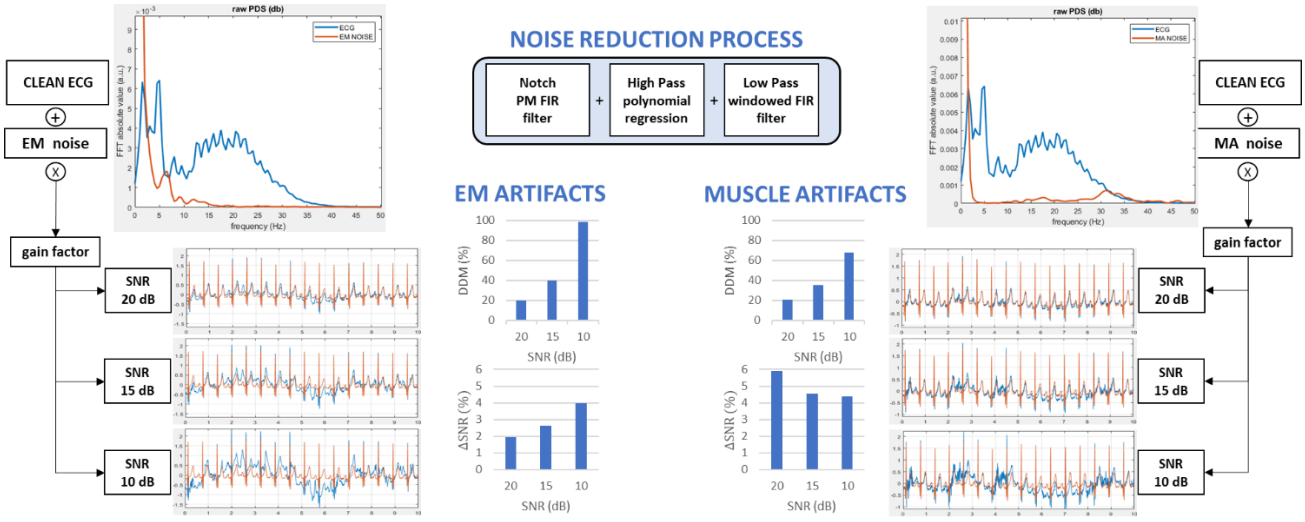

Figure 34

4 QRS DETECTION

The detection of the QRS complex is the most important task in automatic ECG signal analysis. The QRS complex detection is the first step for further ECG examinations including signal quality assessment and heart rate analysis.

The detection of the QRS complex in an electrocardiogram (ECG) signal is a difficult problem since it has a time-varying morphology and can be affected by several noise sources previously described.

In this section two different QRS detection algorithms have been proposed and their characteristics and performances discussed. The first QRS detector is the well known and diffused Pan-Tompkins algorithm; the other is an own implemented QRS detector based on wavelet transforms. These algorithms have different properties and performance specially when dealing with noisy signals. Therefore, it is possible to discover noisy signal by comparing and matching both QRS locations resulted by the two different detectors (Fig. 35). If results are comparable withing a small error, then the ECG signal is classified as good quality and QRS locations are determined. In other cases, in which results are different, ECG signal is classified as bad quality and therefore discarded from successive analysis. More detailed information about the Signal Quality Assessment will be given in the next chapter.

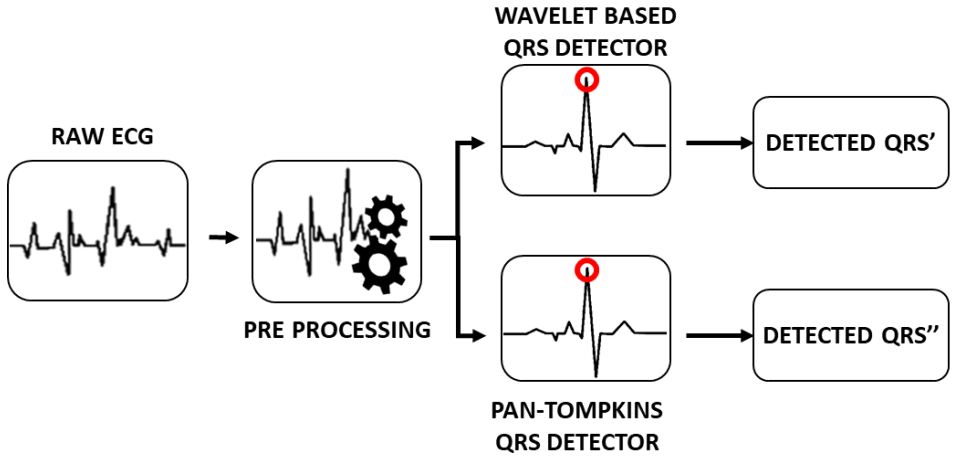

Figure 35

Raw ECG signals are firstly preprocessed so that both QRS detectors algorithms can work on filtered ECG signals with reduced noise content and emphasized QRS complexes. ECG signals are filtered using previously described noise reduction process to which a high pass filter with cut-off frequency 10 Hz was added to reduce T wave prominence and emphasize QRS complex (Fig. 36).

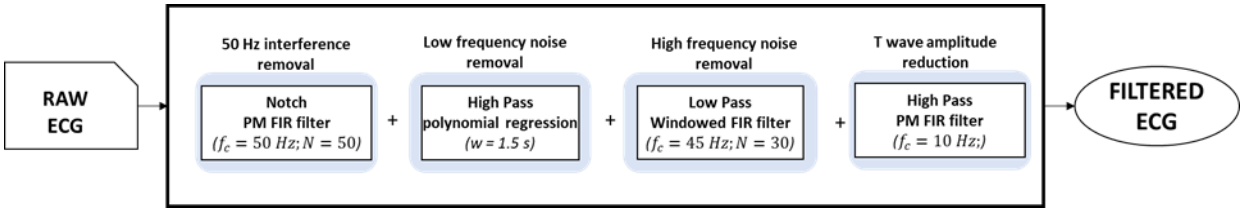

Figure 36

Generally, QRS detector algorithms can be divided into two stages: a first preprocessing stage where the input signal is manipulated and transformed using different techniques. In particular wavelet based QRS detector applies wavelet transform to the input signal, while Pan Tompkins algorithm applies a series of filters to emphasize the QRS complexes. Then, in the decision stage, each algorithm applies decision algorithm based on thresholds to detect R peaks. Moreover, in the decision stage, many settings have to be settled including refractory period that was chosen to be 200 ms so that any peak that occurs within 200 ms from the R-peak is discarded.

Both QRS detection algorithms have been tested using MIT-BHI Arrhythmia database that includes 48 half hours I-lead ECG recording from 47 subjects. This database in commonly used for algorithm performance evaluation.

Moreover, since the aim of this study is focused on application analysis of Vital-ECG watch device that records 10 seconds ECG signal, each ECG signal is windowed using a sliding window 10 seconds long and each ECG window is provided to the input of both QRS detection algorithm.

4.1 WAVELET BASED DETECTOR

The algorithm is based on multiresolution wavelet transform which is robust to time varying QRS complex morphology and to noise. Haar wavelet is chosen as “mother” wavelet and scales between 1 to 4 were chosen for the analysis due to spectral characteristics of the electrocardiogram (ECG) signal where high frequency content of QRS complexes are more evident than other ECG waves. Considering each signal is acquired using a sampling rate of 360 Hz, each decomposition level focuses on different frequency bands: the first decomposition level focuses on a frequency band bounded between 90 – 180 Hz; the second level between 45 – 90 Hz; the third level between 22,5 – 45 Hz; the fourth level between 11,25 – 22,5 Hz.

Starting from the last decomposition level and progressing towards the first level, a peak detection process is applied for each level. It is important to know that the maxima and minima points of the decomposed signal correspond to the zero crossing points of the original signal so that each R wave can be delimited within its zero crossing points.

The maxima and minima points of the decomposed signal are localized with a threshold-based searching algorithm that uses global thresholds computed considering whole 10 seconds ECG windowed signal, and local thresholds computed on an overlapping sliding window 1 second long (Fig. 37). The sliding window of 1 second width is moved with an overlap of 200 ms corresponding to the refractory period settled by user settings.

In each sliding window the maxima and minima peaks that are respectively greater than the upper and lower global and local thresholds are detected. The analysis of several decomposition levels starting from larger scale towards the finest scale allows to manage the presence of noises that can corrupt ECG records resulting in false peak detection. The key condition is that the detection process analyzing lower scales only preserves maxima and minima points that match with previously detected points in larger scales. In this way false peaks resulting from low frequency noise effect are deleted when compared to finest scale analysis. Moreover, false peaks resulting from high frequency noise effect are not considered because do not match with previously detected points in lower scales.

The analysis of the decomposition levels is computationally expensive and, to reduce time consuming, it proceeds until matching of maxima and minima points are founded between two consecutive levels. Finally, R peaks are detected in the range determined by the zero crossing points.

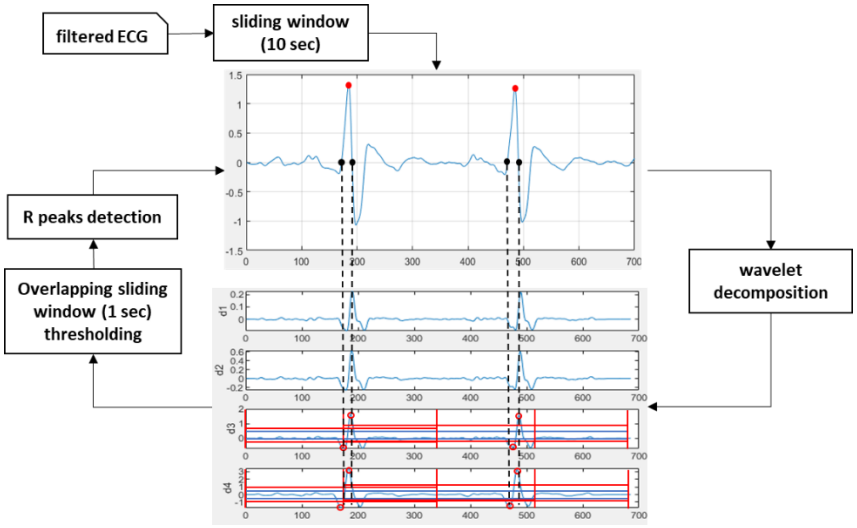

Figure 37

Threshold levels play vital role in QRS detector algorithm and it is important to choose most appropriate threshold level. Both global and local thresholds are specular around zeros to allow maxima and minima points detection. The global threshold settled to be very low for lower amplitude false peak removal and it is computed using a small factor as a percentage of maxima and minima ECG value respectively. Local threshold, on the contrary is settled to have a great discriminating effect and is computed using doubled value of global multiplicative factor on maxima and minima ECG value within 1 second sliding window. In this way, by settling global threshold percentage, local threshold is automatically defined.

4.2 PAN TOMPKINS DETECTOR

The Pan–Tompkins algorithm is commonly used to detect QRS complexes.

The algorithm first applies a series of filter to emphasize extremely sharp and fast signal variation that characterize QRS complexes and to reduce noise effects that contaminate the signal (Fig. 38). Starting from the previously filtered signal, the algorithm applies a derivative filter, then squares the signal and finally integrates the signal using a moving window 20 ms long. In this way, the algorithm highlights QRS complexes and reduce T wave prominence. Finally, the algorithm thresholds the integrated signal to detect the region above the threshold value. Threshold values are computed as a percentage of the signal energy. The algorithm localizes the regions of the integrated signal greater than threshold value and then detects R peaks in the original signal searching the highest peak in each localized region.

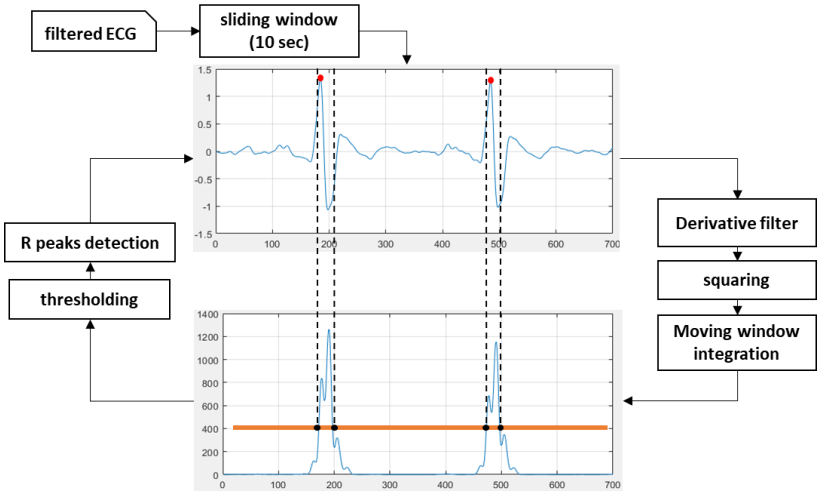
filtered ECG
sliding window
(10 sec)
Derivative filter
squaring
Moving window
integration
R peaks detection
thresholding

Figure 38

4.3 QRS DETECTORS PERFORMANCES

The choice of optimal threshold level is important to optimize QRS detection performance. By using the MIT-BHI arrhythmia database several thresholds values have been tested for both algorithms (Fig. 39). By using smaller thresholds, detection algorithms are more sensible to detect smaller peak of the signal. On the other hand, by using greater thresholds, more specific and less sensible detections are obtained.

Considering wavelet-based detection algorithm, by comparing performances of different threshold values it is evident that best results occurs using global thresholds equal to 0,15% of maxima and minima values. Detailed results of wavelet-based detector performance on MIT-BHI arrhythmia database are available in appendix B.

Considering Pan-Tompkins algorithm, by comparing performances of different thresholds values it is evident that best results occurs using threshold level equal to 0,2 % of the energy content of the signal. Detailed results of Pan-Tompkins detector performance on MIT-BHI arrhythmia database are available in appendix C.

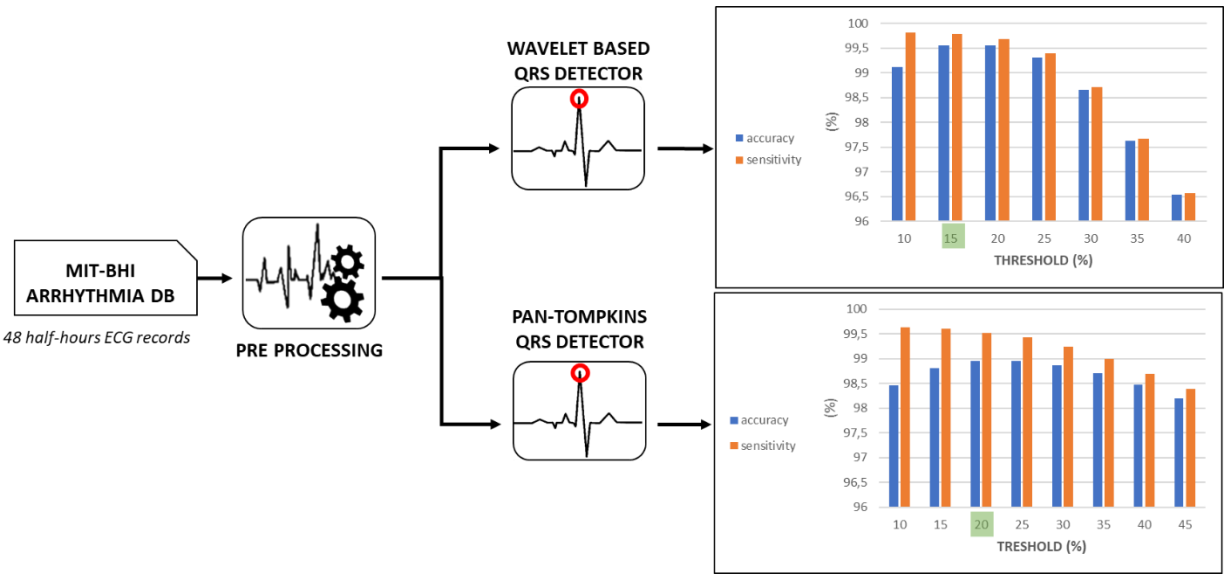

Figure 39

5 SIGNAL QUALITY ASSESSMENT

ECG signal quality assessment (SQA) plays a vital role in significantly improving the diagnostic accuracy and reliability of unsupervised ECG analysis systems. The presence of noise and artifacts can produce large errors in the estimation of characteristics of signals values, leading to false alarms in detection of QRS complexes and therefore corrupting heart rate variability signal on which AF detection is based.

In order to increase ECG analysis performances, a noisy signals detection process based on SQA algorithm has been introduced to detect and discard bad quality signals that are not adequate to be correctly processed. The SQA algorithm relies upon three principal conditions associated to a low-quality signal including signal saturation level, missed QRS complex and false detected QRS complexes (Fig. 40).

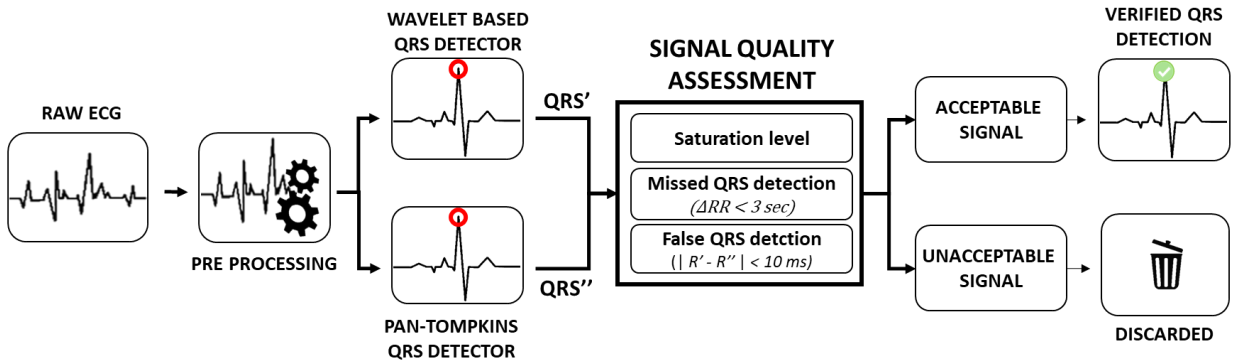

Figure 40

The signal saturation level condition focuses on the amplitude signal dynamics and detect abrupt amplitude variations caused by noises and artifacts that can lead the signal to saturate. When the saturation level is reached, the signal is classified as unacceptable.

The missed QRS complexes condition is based on QRS detection algorithms results. The RR time intervals are analyzed to verify that RR intervals do not exceed a settled maximum threshold of 3 seconds. If the threshold is exceeded, the signal is classified as unacceptable because of probable missed QRS detection.

The false detected QRS complexes condition is the most important condition to improve performances of noisy signals detection process. The key idea is to apply both QRS detection algorithms previously described and compare their results. A good quality signal lead to comparable identical QRS detection results within 10 ms precision range, while results differs more than 10ms precision range considering too noisy signals which quality is not sufficient to provide accurate results and therefore, are classified as unacceptable.

This last condition relies upon different QRS detection algorithm characteristics and properties in managing noise and artifacts corrupting analyzed signals. By using respectively the previously selected thresholds, each algorithm was tested using the MIT-BHI Noise Stress Database that include 2 minutes of calibrated amount of EM artifacts added to a 30 minutes long clean signal in order to obtain specific SNR levels (Fig. 41). It is evident that for lower SNR ratio, algorithms accuracy decrees due to false positive peaks and missed peaks more rapidly in Pan-Tompkins algorithm than in Wavelet-based algorithm. Considering sensitivity performances that measures only missed peaks ratio, Pan Tompkins algorithm achieves higher sensitivity levels even with lower SNR ratio.

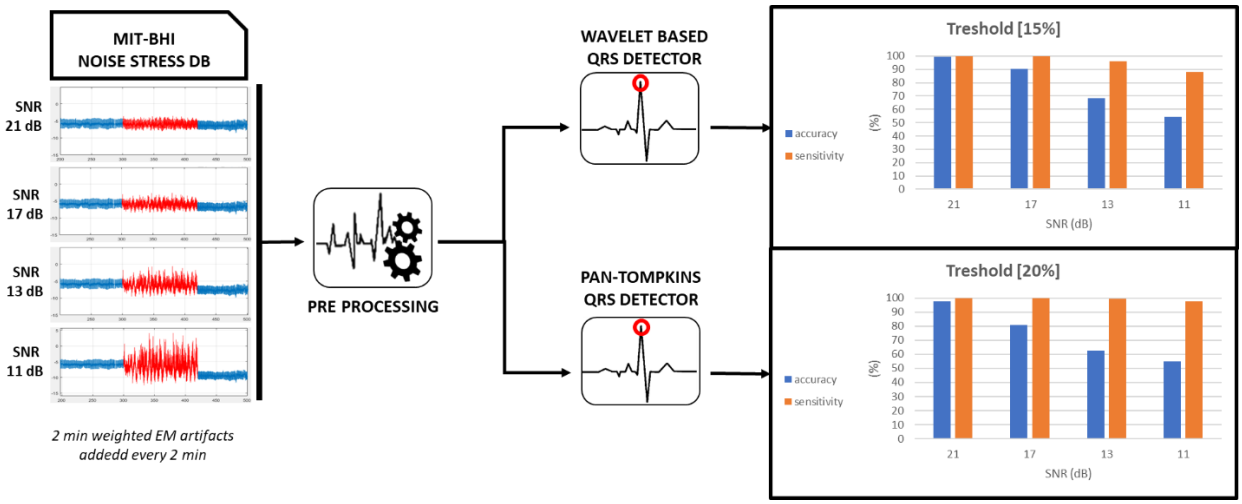

Figure 41

By analyzing and comparing performances trend of both algorithms, their different characteristics in managing noises are evident. Wavelet-based algorithm appears to be more specific and more robust against false peaks detections than Pan-Tompkins algorithm that, in contrast, is more sensible to detect peaks but also to detect false positive peaks.

By combining both algorithms properties, it is possible to detect noisy signals by comparing both QRS detected complexes and searching for differences among results. Good quality signals are expected to return identical results for both algorithms. Noisy signals, on the contrary, can generate same differences in false peaks detection or missed peaks.

5.1 SQA PERFORMANCES

The reliability of SQA system has been evaluated using the MIT-BHI Noise Stress Database that include a 30 minute long clean signal from MIT-BHI Arrhythmia Database corrupted by 2 minutes of calibrated amounts of EM artifacts added every 2 minutes. In order to study the sensibility of noise detection, several SNR levels corresponding to several amount of noise have been considered (Fig.42).

Each signal have been windowed using 10 seconds non overlapping sliding window. Each windowed signal has been analyzed with both QRS detection algorithms and their results have been used in the SQA process that classifies each window as acceptable or not acceptable. Good noise detection performance are achieved with lower SNR ratio when all windows belonging to 2 minutes added noise are correctly classified as unacceptable. For higher SNR ratio, noise effects are less evident and therefore more difficult to be detected.

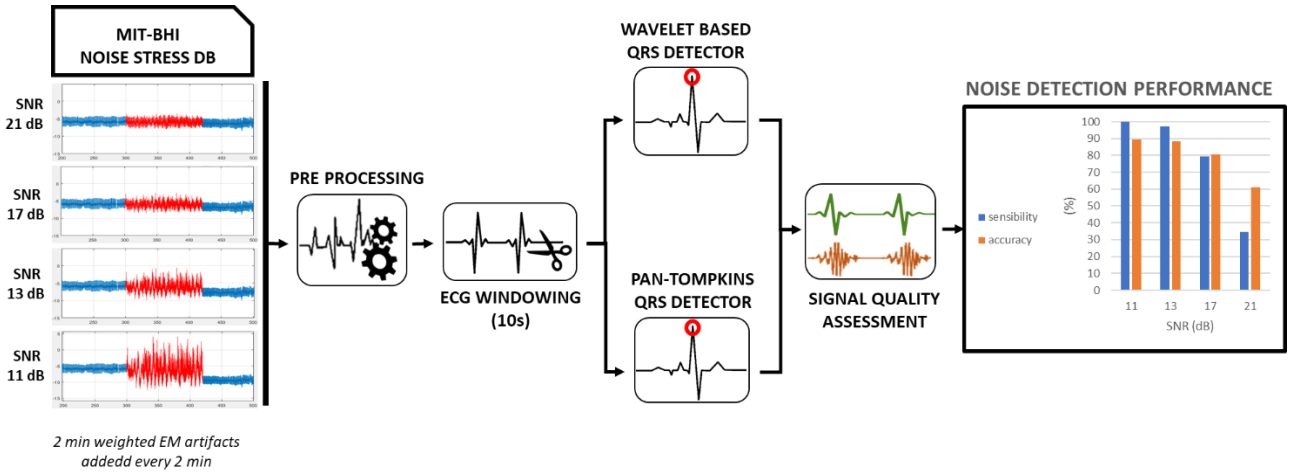

Figure 42

6 AF DETECTION ALGORITHM

In this chapter a new original atrial fibrillation (AF) detection algorithm is described, and its classification performances are then discussed. The algorithm is based on heart rate variability (HRV) signal that is one of the mostly used methods for assessing the heart activity and discrimination of cardiac abnormalities. The HRV is a nonlinear and nonstationary signal that represents the autonomic activity and its influence on the cardiovascular system. It is extracted from time RR intervals between consecutive peaks and, therefore, exact R peak detection is essential to correctly extract HRV signals.

HRV allows AF detection because AF is characterized to be “irregularly irregular” heart rhythm that consequently increases both variability and complexity of HRV signal. For unquestionable diagnosis of the atrial fibrillation, atrial activity analysis is essential, but a stable, high quality signal without extensive noise is required for the analysis, which is hardly achievable by portable single lead ECG monitoring. Therefore, P wave detection process is currently not considered.

The proposed automated AF detection algorithm (Fig.43) is composed by two classification stages. In the first step, ECG signals are firstly decomposed in 5 beats ROI (region of interest) from which a set of HRV features are extracted and are then cleaned and reduced to improve classification that is achieved using MLP (Multi Layer Perceptron) NN. The NN output is a linear function that is used in the second classification step after an appropriate transformation. In particular, the post process maps classified ROI into 256 grey scale and each ECG ROI sequence is transformed into a grey-scale image where each ROI corresponds to a pixel. In the image classification process, several features are extracted from grey-level images and are then cleaned and reduced to improve classification that is achieved with a MLP NN that classifies the ECG record into NSR of AF class.

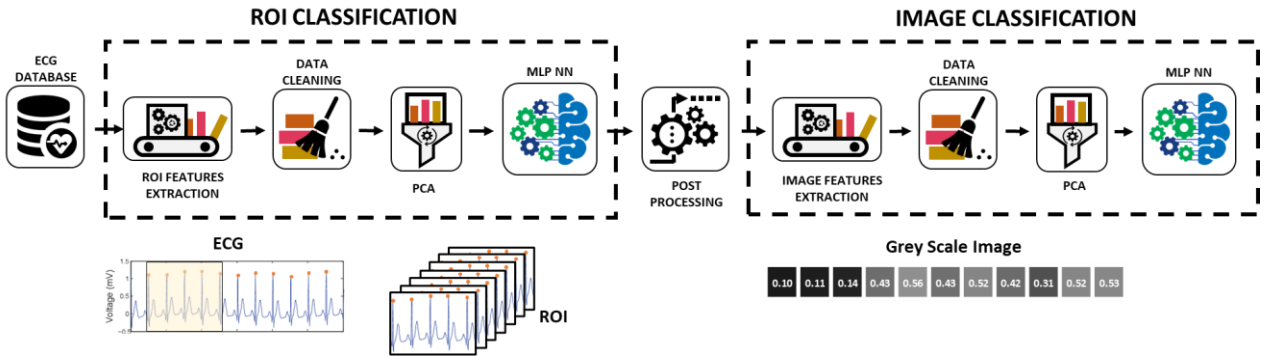

Figure 43

6.1 ECG DATABASED CONSTRUTION

The AF algorithm has been trained and tested starting from an ECG database built of AF events and NSR events extracted from several MIT-BHI annotated databases including MIT-BHI arrhythmia database, long term AF database (ltafdb) and AF database (afdb) (Fig.44).

These databases include long-term ECG recordings of 156 patients with paroxysmal or sustained AF episodes diagnosed by expert cardiologists annotating start and stop indexes of each AF episode. Only AF episodes between 30 and 120 seconds have been considered for this study to reduce the risk of intermittent NSR events into a longer AF annotated episode that may led to validity corruption of data. Moreover, only NSR events longer than 120 seconds have been considered because shorter episode may be characterized by instable rhythm.

The selected ECG episode are then windowed with 10 seconds window long to emulate VITAL-ECG recordings. Each ECG window is pre-processed and its QRS complexes detected with both wavelet based and Pan-Tompkins algorithms that are used in the signal quality assessment process to detect and discards too noisy records that cannot be processed. The ECG database has been constructed using only acceptable quality records. The constructed ECG database include 25 h recording AF rhythm and 25 h recording NSR rhythm belonging to 68 patients.

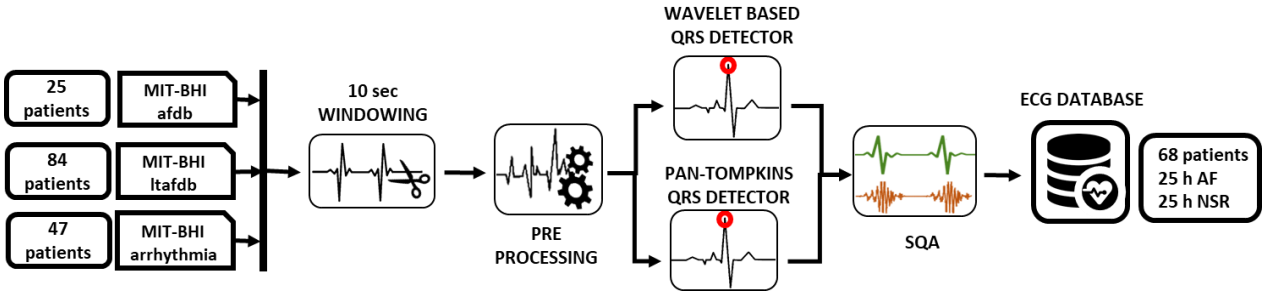

Figure 44

6.2 ROI CLASSIFICATION

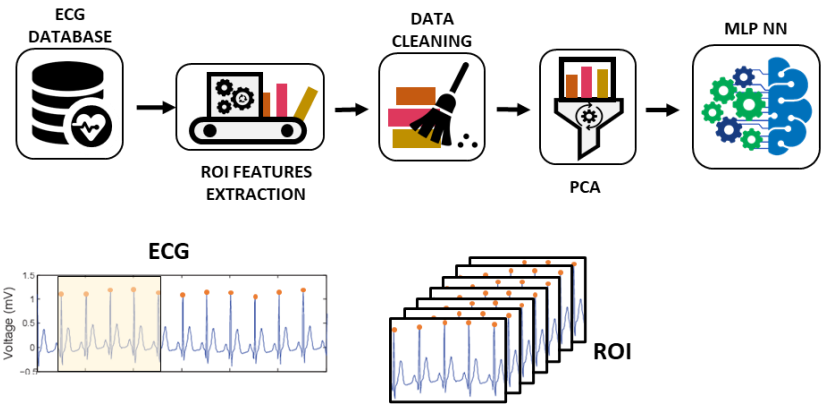

Figure 45

6.2.1 FEATURES EXTRACTION

Starting from the ECG database previously constructed, each record has been decomposed in a sequence of 5 beats ROI from which 47 HRV features have been extracted. These features can be generally divided in linear and non-linear features. The cardiovascular system is too complex to be linear and treating it as a non-linear system can lead to better understanding of the system dynamics. Linear features include time, geometrical and frequency-based analysis. Non-linear features include geometrical and entropy measures. The combination of linear and non-linear features has been used.

Time domain measures is the simplest method to perform RR interval analysis. The series of RR intervals can also be converted into a geometric pattern model and several metrics can be used to judge the variability based on the geometric and graphic properties of the resulting pattern. In this study two geometrical approaches have been used including Poincare plot and histogram-based analysis.

Spectral analysis is the most popular linear technique used in the analysis of HRV signals because frequency-domain analysis provides for the separation of parasympathetic (high-frequency range) and sympathetic activity (low frequency range) signals.

Entropy analysis metrics are valuable in the assessment of HRV signal, because ‘‘hidden information’’ related to underlying mechanisms can be obtained.

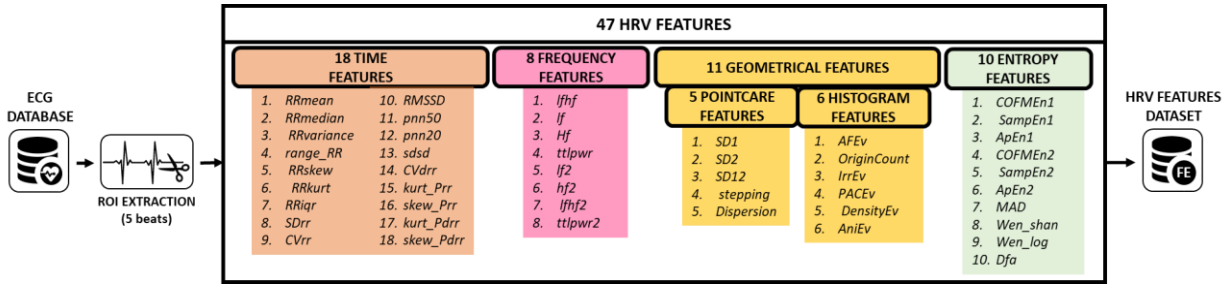

Figure 46

TIME DOMAIN FEATURES

With time domain metrics either the heart rate at any point in time or the intervals between successive QRS complexes are determined.

- **Features based on RR interval**

1. *RRmean* *(ms) mean value of RR intervals*
2. *RRmedian* *(ms) median value of RR intervals*
3. *RRvariance* *(ms) variance of RR intervals*
4. *range_RR* *(ms) max (RR) – min (RR)*
5. *RRskew* *(a.u.) skewness of RR interval distribution*
6. *RRkurt* *(a.u.) kurtosis of RR interval distribution*
7. *RRiqr* *(ms) interquartile range (IQR) that measures statistical dispersion, being equal to the difference between 75th and 25th percentiles.*
8. *SDrr* *(ms) Standard deviation of RR intervals.*
9. *CVrr* *(a.u.) coefficient of variation of RR, computed as the variance normalized by the mean value of RR intervals.*

- **Features based on diff (RR)**

10. *RMSSD* *(ms) The square root of the mean of the sum of the squares of differences between adjacent RR intervals.*
11. *pnn50* *(%) Number of pairs of adjacent RR intervals differing by more than 50 ms divided by the total number of all RR intervals.*
12. *pnn20* *(%) Number of pairs of adjacent RR intervals differing by more than 20 ms*
13. *sdsd* *(ms) variance of the difference of adjacent RR intervals.*
14. *CVdrr* *(a.u.) coefficient of variation of difference of adjacent RR intervals*

- **Features based on the *Estimated* probability Density of RR intervals**

15. *kurt_Prr* *(a.u.) kurtosis of the estimated probability density of RR intervals*
16. *skew_Prr* *(a.u.) skewness of the estimated probability density of RR intervals*

- **Based on the estimated probability Density of diff (RR)**

17. *kurt_Pdrr* *(a.u.) kurtosis of the estimated probability density of differences of adjacent RR*

intervals

18. *skew_Pdrr* *(a.u.) skewness of the estimated probability density of differences of adjacent RR intervals*

FREQUENCY DOMAIN FEATURES

Spectral analysis is the most popular linear technique used in the analysis of HRV signals. Frequency-domain analysis (Fig. 47) provides for the separation of parasympathetic (high-frequency range) and sympathetic activity (low frequency range) signals. Spectral power in the high-frequency (HF) (0.15-0.5 Hz) band reflects respiratory sinus arrhythmia and thus cardiac vagal activity. Low-frequency (LF) (0.04-0.15Hz) power is related to baroreceptor control and is mediated by both vagal and sympathetic systems.

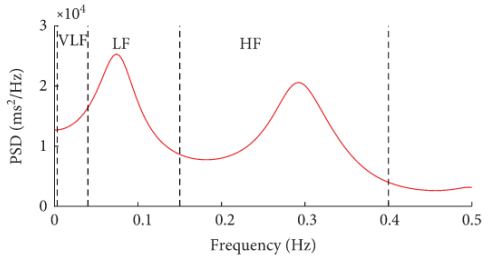

Figure 47

The power spectral density (PSD) can be calculated with parametric and non-parametric methods. Non-parametric methods do not need stationary sampling frequency signals and they are mostly used for HRV signal analysis because of its non-stationary nature. On the contrary parametric methods need the signal to be stationary and therefore a non-stationary signal makes the PSD instable.

In this study both parametric and non-parametric methods have been used to compute PSD and frequency features have been extracted from both PSD. The parametric PSD is estimated with Burg method that fits an autoregressive (AR) model to the signal by minimizing (least-squares) the forward and backward prediction errors while constraining the AR parameters to satisfy the Levinson-Durbin recursion. The non-parametric PSD is estimated using the Lomb-Scargle periodogram that is computed using a sampling frequency determined by the maximal frequency detected in RR intervals.

- **FREQUENCY FEATURES BASED ON PARAMETRIC POWER SPECTRAL DENSITY ESTIMATED WITH BURG METHOD**

1. *ttlpwr* *(ms^2) Total spectral power (approximately <0.4 Hz)*
2. *lf* *(ms^2) Power in low frequency range (0.04Hz <= lf < 0.15 Hz)*
3. *hf* *(ms^2) Power in low frequency range (default 0.15Hz <= hf < 0.4 Hz)*
4. *lfhf* *Ratio LF [ms^2]/HF [ms^2]*

- **FREQUENCY FEATURES BASED ON LOMB-SCARGLE PERIODOGRAM METHOD**

5. ttlpwr2 *(ms^2) Total spectral power (approximately <0.4 Hz)*
6. *lf2* *(ms^2) Power in low frequency range (0.04Hz <= lf < 0.15 Hz)*
7. *hf2* *(ms^2) Power in low frequency range (default 0.15Hz <= hf < 0.4 Hz)*
8. *lfhf2* *Ratio LF [ms^2]/HF [ms^2]*

GEOMETRICAL FEATURES

POINCARE BASED FEATURES

Poincare plot is a technique taken from non-linear dynamics and portrays the nature of R-R interval fluctuations showing each R-R interval plotted against the next interval. Poincare plot analysis is an emerging quantitative-visual technique whereby the shape of the plot is categorized into functional classes that indicate the degree of heart failure in a subject. The plot provides summary information as well as detailed beat-to-beat information on the behavior of the heart.

The Poincare plot can be analyzed quantitatively by calculating the standard deviations of the distances of the R-R(i) to the lines y = x and y = -x + 2*R-R_m, where R-Rm is the mean of all R-R(i). The standard deviations are referred to as SD1 and SD2, respectively. SD1 related to the fast beat-to-beat variability in the data, and SD2 described the longer-term variability of R-R(i). The ratio SD1/SD 2 can also be computed to describe the relationship between these components.

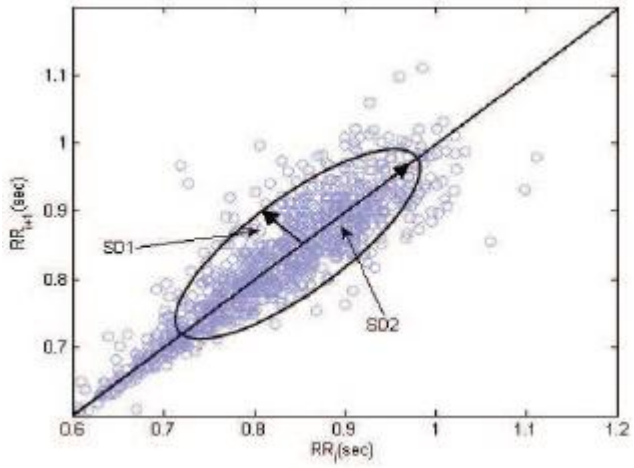

Figure 48

1. *SD1* *(ms) Standard Deviation of the projection of PP on the line perpendicular to the line of identity (y=-x) which characterizes the short-term HRV. It measures the width of Poincare cloud.*
2. *SD2* *(ms) Standard Deviation of the projection of PP on the line perpendicular to the line of identity (y=x) which characterizes the long-term HRV. It measures the length of the Poincare cloud.*
3. *SD12* *(ms) SD1 / SD2 ratio*

4. *Stepping* *Mean Stepping Increment of Inter Beat Intervals*
5. *Dispersion* *Dispersion of points around central point on the diagonal line*

HISTOGRAM BASED FEATURES

The δRR interval, defined as δRR(i) = RR(i) - RR(i-1), is a measure of irregularity. The Lorenz plot of δRR intervals, which is a scatter plot of δRR(i - 1) versus δRR(i), encodes the uncorrelated nature of RR intervals in the direction of change of three consecutive RR intervals.

The 2-D histogram is a numeric representation of a Lorenz plot with bins of size binSize and 13 regions of the histogram (sequences) have been defined and characterized (Fig.49). The δRR interval distribution is studied by analyzing bin counts in each sequence. For example, during normal sinus rhythm (NSR), bins within segment 0 of the 2-D histogram are mostly populated, whereas during AF, all segments are populated.

Several evidence-based metrics have been employed to measure δRR distributions, including origin count that measure numbers δRR populating the origin segment; irregularity evidence (IrrEv), density evidence (DensityEv), anisotropy evidence (AniEv), premature atrial contraction evidence (PACEv). Finally, atrial fibrillation evidence (AFEv) is computed as linear combination of all these evidence-based metrics.

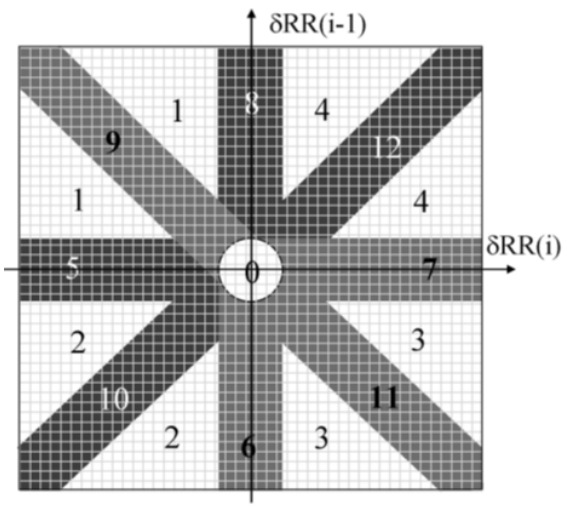

(a)

Segments	Sequence	δRR Values
0	SSS/LLL	$\lvert\delta RR\rvert < \text{NSRmask}$
1	S-L-S	$\lvert\delta RR(i-1)\rvert \neq \lvert\delta RR(i)\rvert$
2	L-M-S	$\lvert\delta RR(i-1)\rvert \neq \lvert\delta RR(i)\rvert$
3	L-S-L	$\lvert\delta RR(i-1)\rvert \neq \lvert\delta RR(i)\rvert$
4	S-M-L	$\lvert\delta RR(i-1)\rvert \neq \lvert\delta RR(i)\rvert$
5	L-L-S	One $\lvert\delta RR\rvert < \text{NSRmask}$
6	L-S-S	One $\lvert\delta RR\rvert < \text{NSRmask}$
7	S-S-L	One $\lvert\delta RR\rvert < \text{NSRmask}$
8	S-L-L	One $\lvert\delta RR\rvert < \text{NSRmask}$
9	S-L-S	$\delta RR(i-1) \cong -\delta RR(i)$
10	L-M-S	$\delta RR(i-1) \cong \delta RR(i)$
11	L-S-L	$\delta RR(i-1) \cong -\delta RR(i)$
12	S-M-L	$\delta RR(i-1) \cong \delta RR(i)$

(b)

Figure 49

1. OriginCount (a.u.) number of δRR interval within a threshold
2. IrrEv (a.u.) measures the sparseness of δRR distribution
3. PACEv (a.u.) measure the evidence of compensatory pauses
4. DensityEv (a.u.) Density evidence measures the density in a cluster

5. AniEv (a.u.) measures the orientation of the distribution
6. AFEv (a.u.) (IrrEv-OriginCount-2*PACEv)

ENTROPY BASED FEATURES

- **ENTROPY FEATURES BASED ON EMBEDDING DIMENSION (m = 1) AND TOLLERANCE ($r = 0.2 * std$)**

1. *COFMEn1* *(a.u.) coefficient of fuzzy measure entropy*
2. *SampEn1* *(a.u.) sample entropy*
3. *ApEn1* *(a.u.) approximate entropy*

- **ENTROPY FEATURES BASED ON EMBEDDING DIMENSION (m = 2) AND TOLLERANCE (r = 0.2*std)**

4. *COFMEn2* *(a.u.) coefficient of fuzzy measure entropy*
5. *SampEn2* *(a.u.) sample entropy*
6. *ApEn2* *(a.u.) approximate entropy*

- ***OTHER ENTROPY BASED FEATURES***

7. *Wen_shan* *(a.u.) Shannon entropy of wavelets*
8. *Wen_log* *(a.u.) logarithm energy entropy of wavelets*

- ***OTHER NON-LINEAR FEATURES***

9. *MAD* *(ms) median absolute deviation*
10. *Dfa* *(a.u.) DetrendedFluctuation Analysis*

6.2.2 ROI DATA CLEANING

Starting from the feature-based dataset previously extracted, the first essential step for further data analysis include missing values removal. In particular, non-linear entropy measurements can result in Nan values if analyzed HRV signal do not compliant some basic requirements.

Data cleaning process manage missing values is a smart way to both preserve the greatest number of elements and features. Data cleaning process analyzes one by one each feature and searches for missing values (Fig.50). If the number of Nan values are greater than 2% of dataset size then the feature is removed, otherwise elements are removed.

Finally, 1 feature has been removed including Sample entropy measure computed with embedding dimension (m=2). In addition 5 records have been removed.

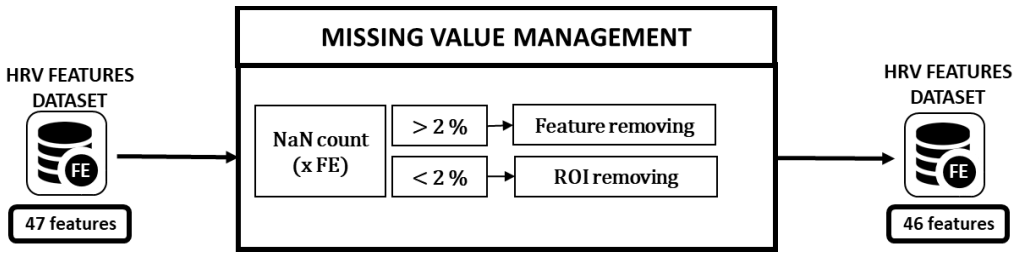

Figure 50

6.2.3 ROI DATA DIMENSIONALITY REDUCTION

Starting from clean dataset containing 46 extracted features, the dimensionality reduction play an important role to improve classification performances because in the reduced space the classification can be done more accurately than in the original space.

Generally, dimensionality reduction of multivariate data represents a powerful method for highlighting more relevant features for the system description and deleting those attribute that are not predictive of the final state of the system (irrelevant) or highly correlated with other variables (redundant). A feature can be defined relevant if it is essential to obtain good predictive performances of the system, otherwise it is irrelevant. Usually, feature relevance can be considered strong if it cannot be removed from the dataset without resulting in a loss of predictive accuracy. On the contrary, feature relevance can be considered weak if it may sometime contribute to predictive accuracy, but this depends on which features are considered. Features are considered informative if they are highly correlated with the decision concept but are highly uncorrelated among them. Usually, two features can be considered irrelevant when considered individually, but they can be highly predictive when they are considered together.

Dimensionality reduction provides several benefits including improving prediction performance, decreasing model complexity, facilitating data visualization, reducing measurements and storage requirements, and reducing training times.

Two different techniques are available for performing dimensionality reduction on the dataset, including feature selection and feature construction. Feature selection simply selects a minimal number of relevant and informative features from the initial set of variables so that the amount of information with respect the original variables is kept intact, and the meaning of features is preserved. Feature construction transforms the data from the high-dimensional space to a new space of fewer dimensions. Feature construction generates a completely new set of features from the original ones through a linear transformation such as Principal Component Analysis (PCA). Generally, PCA is based on extracting the axes on which data shows the highest variability through linear transformation. After the new features has been created, it is important to select the best subset of orthogonally transformed features which allow achieving the best classification.

In this study, dimensionality reduction process has been achieved in two steps including feature filter techniques and PCA feature construction (Fig.51).

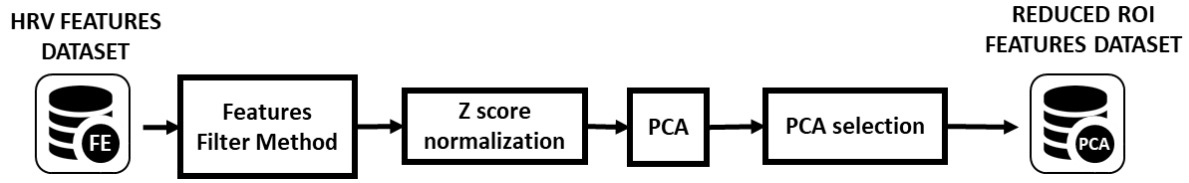

Figure 51

6.2.3.1 FEATURES FILTER METHOD

Filters methods are usually low computationally intensive, and they produce a general feature set useful for exposing features relevance and predictivity of the model. The filter method provides a feature ranking rather than an explicit best feature subset.

Filter method selects the features by ranking them on how useful they are for the model. To compute the usefulness score statistical test and correlation results are used. In particular, the filter method remove most correlated (redundant) features preserving those with higher area under ROC curve. The correlation threshold was settled to 99 %, and 5 features was removed from the dataset. The ROC curve of remaining features is shown in Fig. 52.

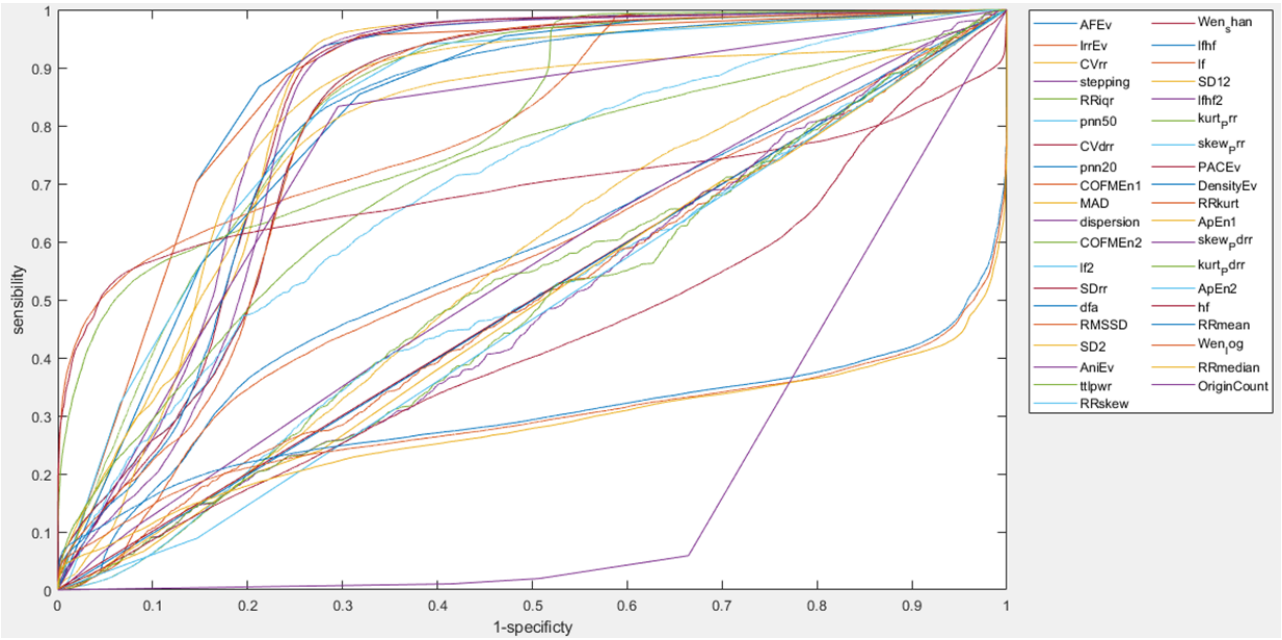

Figure 52

6.2.3.2 FEATURES CONSTRUCTION - PCA

Working with the 41 remaining features, PCA transforms the data from the high-dimensional space to a new space of fewer dimensions. Feature construction generates a completely new set of features from the original ones through a linear transformation such as Principal Component Analysis (PCA). Generally, PCA is based on extracting the axes on which data shows the highest variability through linear transformation. After the new features has been created, it is important to select the best subset of orthogonally transformed features which allow achieving the best classification.

The selection of most relevant principal components has been done with a threshold technique based on eigenvalues that is proportional to the variability of each components. Only the first 20 components with eigenvalues higher than 1 have been selected (Fig. 53).

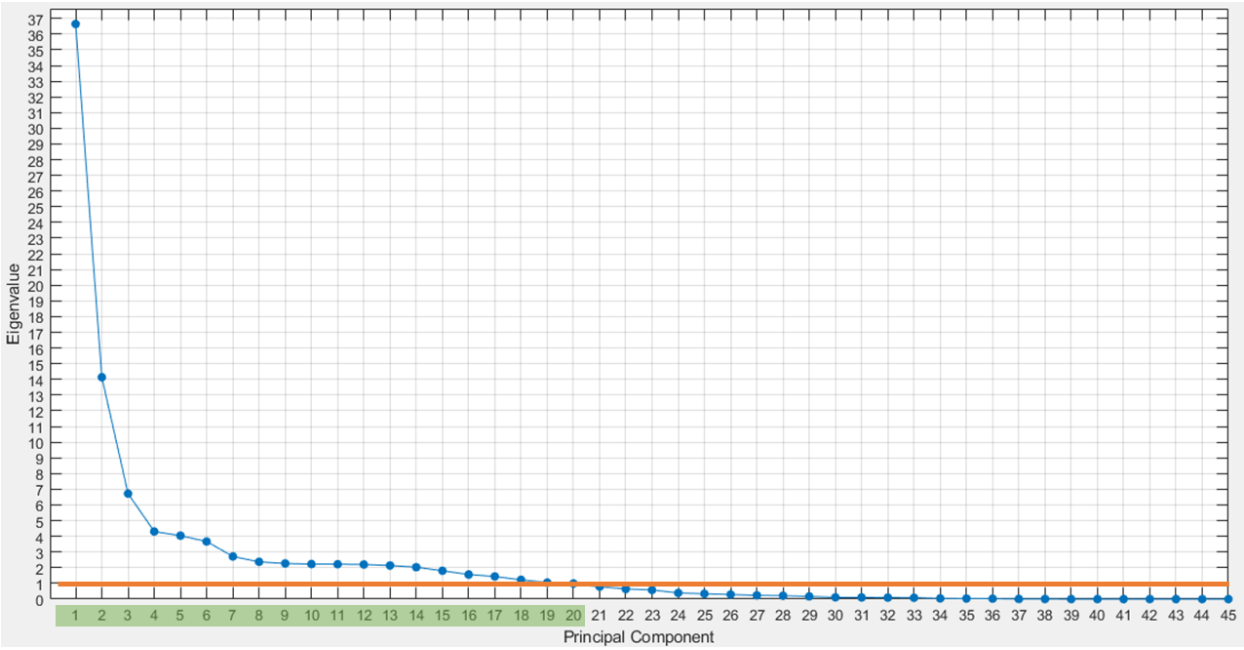

Figure 53

6.2.4 ROI CLASSIFICATION MLP NN

ROI classification process has been applied on the PCA dataset containing 20 selected principal components and generally composed by 50 hours of ECG recording equally balanced into AF and NSR episodes (Fig.54). ECG records are related to 68 different patients and they have been stratified into 5 clusters containing approximatively 5 hours of AF records and 5 hours of NSR records each.

ROI classification has been achieved using several different feedforwards multilayer perceptron (MLP) neural network (NN) triangular configuration from 1 to 3 hidden layers. The number of neurons in the first hidden layer was ranged from 10 to 50 with steps of 10, and the number of neurons were halved for each addition hidden layer to obtain triangular configurations with fixed proportionality dimensions.

Each MLP NN architecture configuration has been trained with a balanced training set composed by 4 clusters of patients containing the same number of elements between the two class that approximately are 20 hours AF records and 20 hours NSR records. NNs have been tested with the remaining cluster of patients that has been used as testing set. Each NN architecture has been trained and tested 5 time for statistical validation since NN weight initialization is random.

Classification performances of each NN architecture are shown in Fig 55. It is evident that best results (lower variability, higher accuracy) occurs with NN of 1 hidden layer containing 30 neurons.

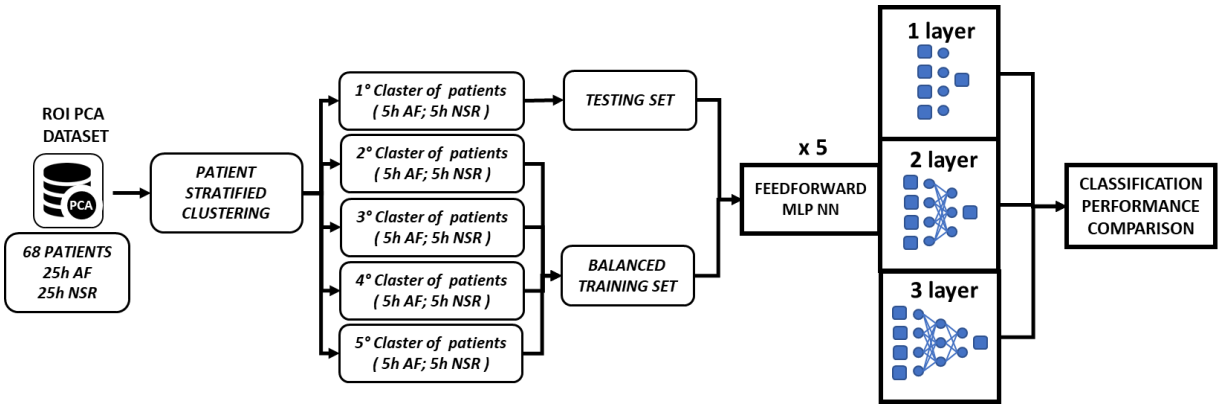

Figure 54

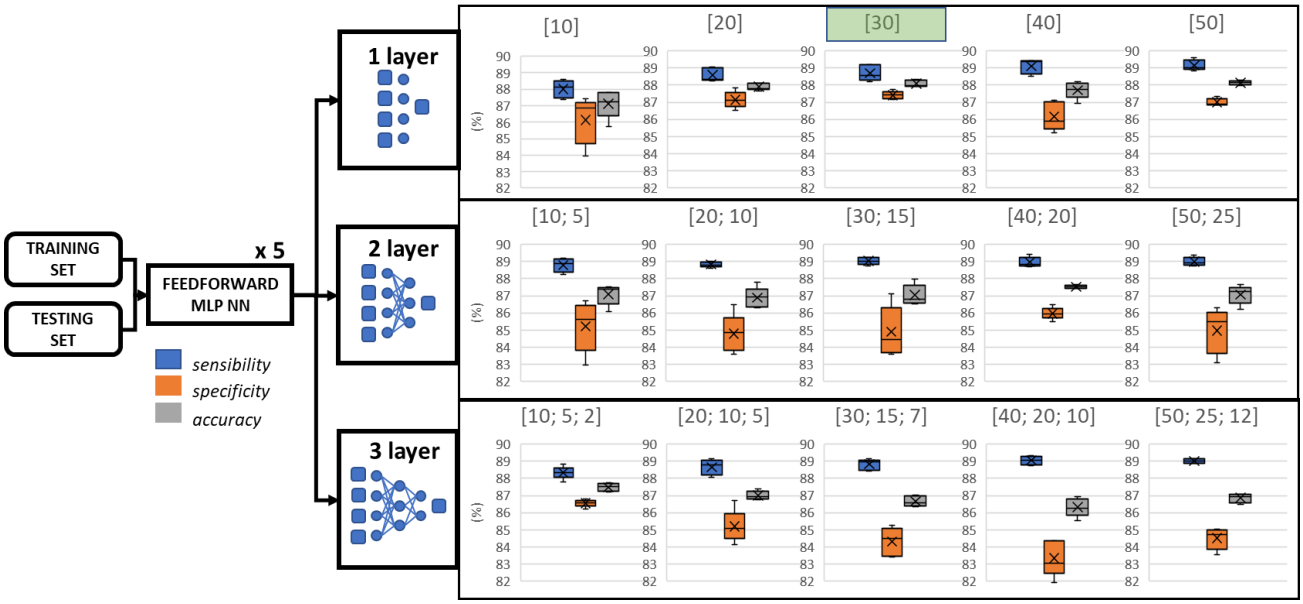

Figure 55

The selected NN configuration (1 hidden layer of 30 neurons) has been validated with 5 fold cross validation technique where iteratively each patient cluster has been used as testing set and remaining clusters used as training set (Fig. 56). At the end of k fold cross validation, all ROI have been classified and each ROI output classification was saved into the classified ROI database.

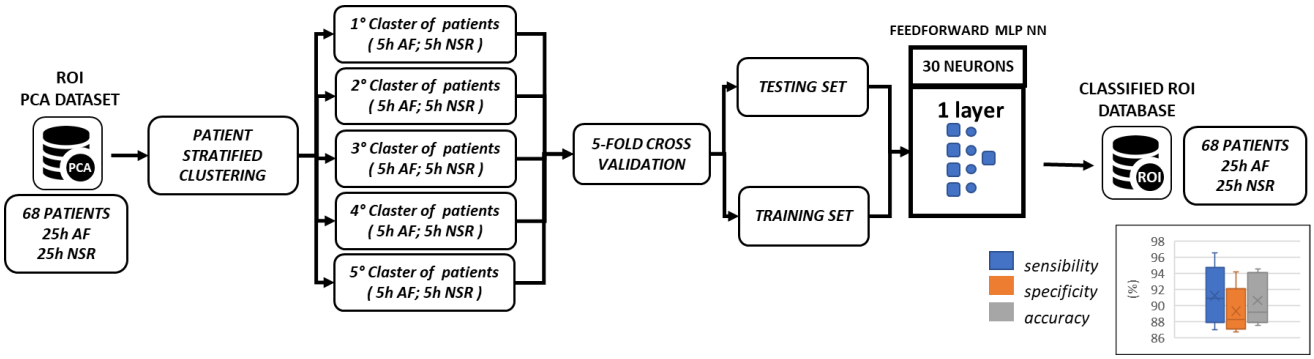

Figure 56

6.3 POST PROCESSING

The classified ROI database contains output values of MLP NN related to each ROI. The NN output neuron is a characterized by a linear activation function and output values distribution are shown in Fig. 57 for both ROI classes. The majority of NSR ROI values are around 0, and most AF ROI output values are around 1. The two classes distribution overlaps in range of values between 0 and 1. Output values greater than 1 are almost all belonging to class 1 and values lower than 0 are almost all belonging to class 0.

In the post processing step, all output values ROIs belonging to each 10 seconds ECG record have been put together to create a sequence of output values that have been mapped to a grey scale image ranged between 0 and 1 using a pixel mapping function in which all values less than 0 are sets to 0 and all values higher than 1 are sets to 1.

The grey level image database contains all 10 seconds ECG records reconstructed as a grey level images where each pixel corresponds to a ROI.

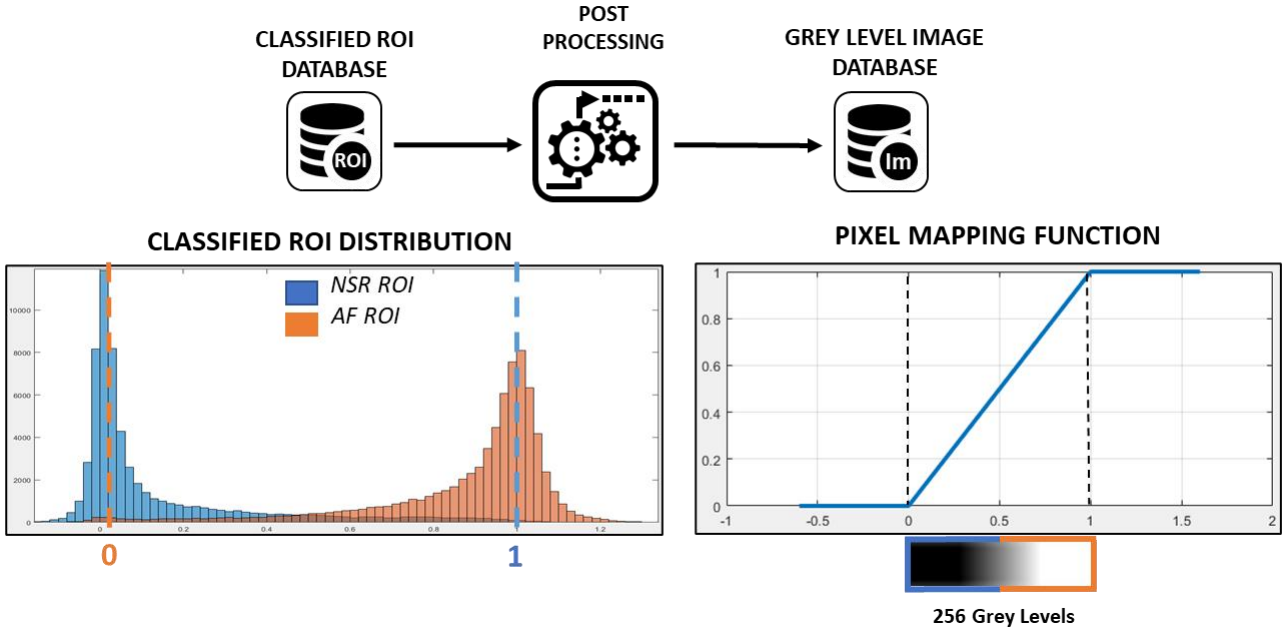

Figure 57

6.4 IMAGE CLASSIFICATION

The grey level image database includes data related to 10 seconds ECG records belonging to 68 different patients from which have been generally extracted 25 hours AF records and 25 hours NSR records (Fig.58).

The classification problem has been resolved with MLP NN features based. A set of features have been extracted from each image and they have been cleaned and reduce to improve classification performances.

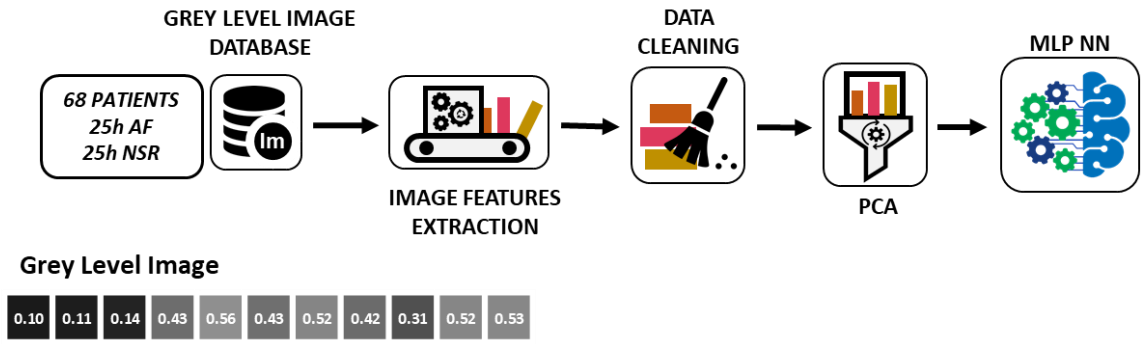

Figure 58

6.4.1 IMAGE FEATURES EXTRACTION

Each ECG record is transformed to a grey scale image where each ROI is a pixel and the luminosity level is equal to ROI output classification value.

Several features have been extracted from images to quantify intensity level pixel distribution (Fig. 59).

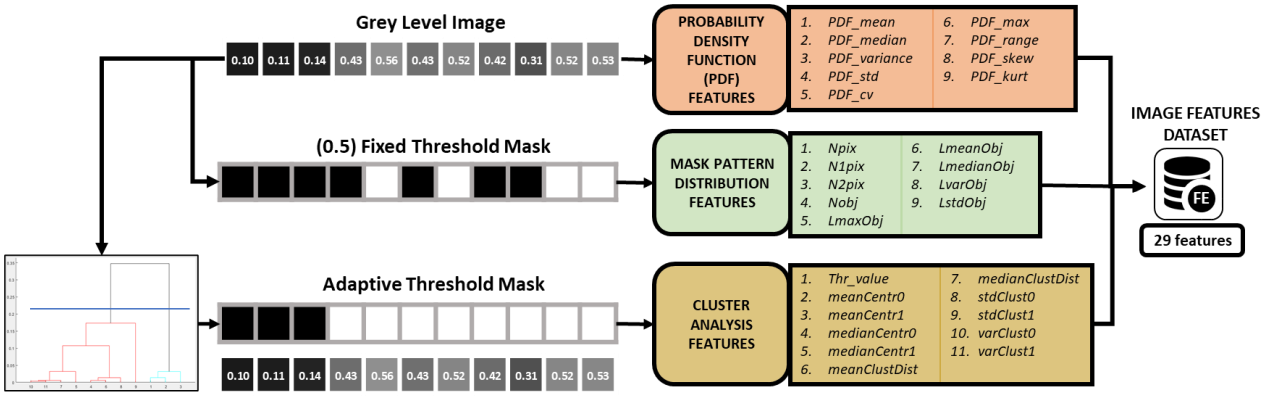

Figure 59

PROBABILITY DENSITY FUNCTION (PDF) FEATURES

From grey-levels images, several features have been extracted considering density probability distribution extracted from intensity pixels histogram.

1. PDFmean → Image pixels intensity mean value

2. PDFmedian → Image pixels intensity median value
3. PDFvar → Image pixel intensity variance
4. PDFstd → Image pixel intensity standard deviation
5. PDFcv → Image pixel intensity coefficient of variation
6. PDFrange → Image pixel intensity range values
7. PDFkurt → Kurtosis of Probability Density Function (PDF)
8. PDFskew → Skewness of Probability Density Function (PDF)
9. PDFmax → pixel intensity of maxima Probability Density Function (PDF)

MASK PATTERN DISTRIBUTION FEATURES

By using 0.5 fixed threshold value, a binary mask has been obtained from each grey level image and a set of features have been extracted from white pixels pattern.

1. Npix → Percentual of all white pixels
2. N1pix →Percentual of isolated white pixels
3. N2pix →Percentual of connected white pixels
4. Nobj →Percentual of connected objects
5. LmaxObj →normalized length of longest object
6. LmeanObj → objects normalized mean length value
7. LmedianObj → objects normalized median length value
8. LvarObj → objects length variance
9. LstdObj → objects length standard deviation

CLUSTER ANALYSIS FEATURES

A set of features have been extracted by two pixels intensity values clusters analysis. Each grey level image has been divided into two cluster using an adaptive threshold obtained from the cutoff value of agglomerative hierarchical cluster tree.

1. Thr_value
2. meanCentr0
3. meanCentr1
4. medianCentr0
5. medianCentr1
6. meanClustDist
7. medianClustDist
8. stdClust0
9. stdClust1
10. varClust0
11. varClust1

6.4.2 IMAGE DATA CLEANING

Generally, 29 features have been extracted from each image and the image features dataset have been formed containing features from all images.

Dataset has been cleaned with the same data cleaning process previously used for ROI features dataset.

Data cleaning process manage missing values is a smart way to both preserve the greatest number of elements and features. Data cleaning process analyzes one by one each feature and searches for missing values (Fig.60). If the number of Nan values are greater than 2% of dataset size then the feature is removed, otherwise elements are removed.

Finally, 1 feature has been removed including the coefficient of variation (cv) of PDF measure.

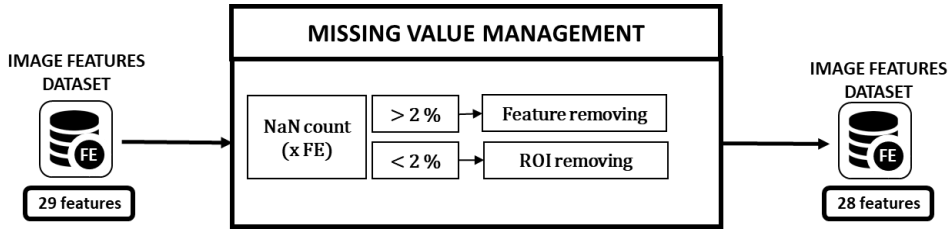

Figure 60

6.4.3 IMAGE DATA DIMESNIONALITY REDUCTION

In this study, dimensionality reduction process has been achieved in two steps including feature filter techniques and PCA feature construction (Fig.61).

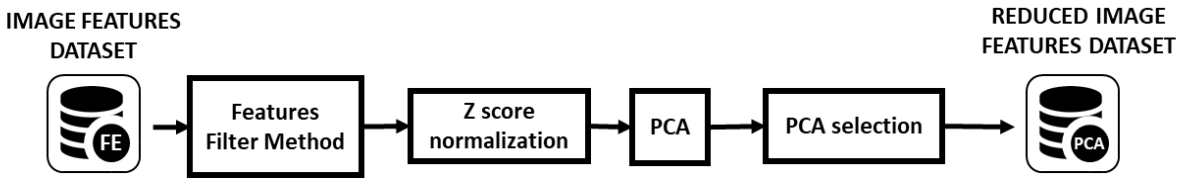

Figure 61

6.4.3.1 FEATURES FILTER METHOD

Filters methods are usually very low computationally intensive, and they produce a general feature set useful for exposing features relevance and predictivity of the model. The filter method provides a feature ranking rather than an explicit best feature subset.

Filter method selects the features by ranking them on how useful they are for the model. To compute the usefulness score statistical test and correlation results are used. In particular ROC operator was used and the filter method removes most correlated (redundant) features preserving those with higher AUC (area under curve). The correlation threshold was settled to 99 %, and 8 features was removed from the dataset. The ROC curve of remaining features is shown in Fig. 62

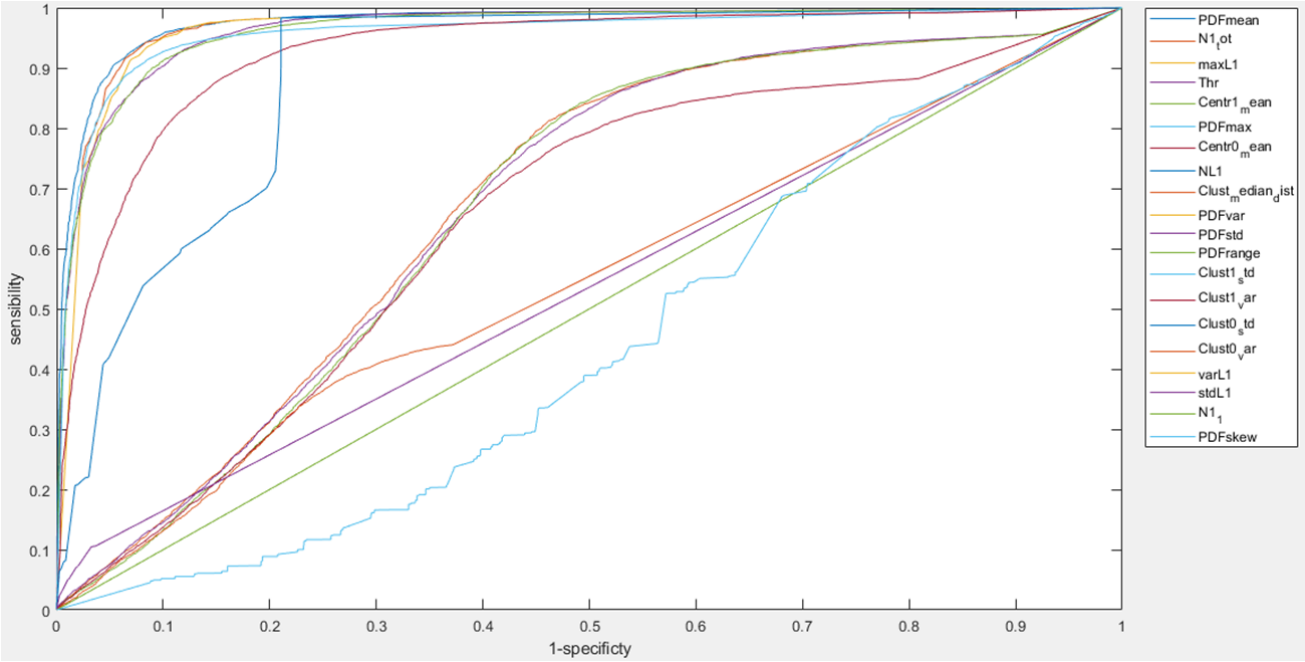

Figure 62

6.4.3.2 FEATURES CONSTRUCTION - PCA

Working with the 20 remaining features, PCA transforms the data from the high-dimensional space to a new space of fewer dimensions. Feature construction generates a completely new set of features from the original ones through a linear transformation such as Principal Component Analysis (PCA). Generally, PCA is based on extracting the axes on which data shows the highest variability through linear transformation. After the new features has been created, it is important to select the best subset of orthogonally transformed features which allow achieving the best classification.

The selection of most relevant principal components has been done with a threshold technique based on eigenvalues that is proportional to the variability of each components. Only the first 8 components with eigenvalues higher than 1 have been selected (Fig. 63).

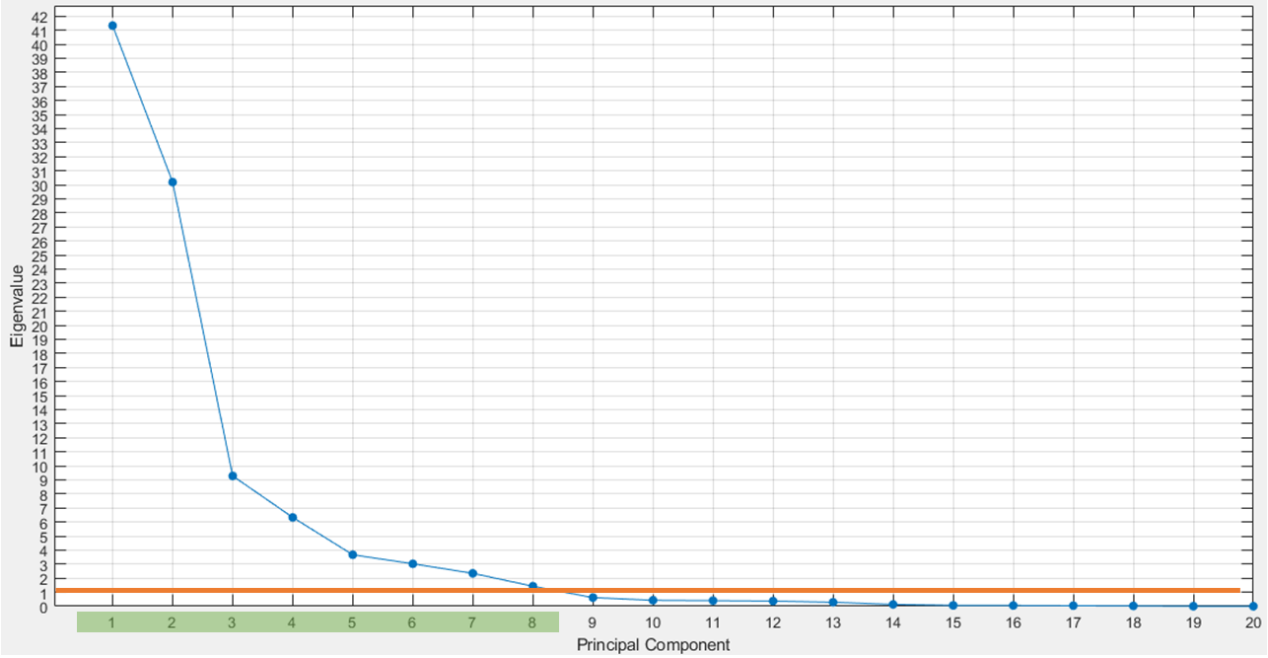

Figure 63

6.4.4 IMAGE CLASSIFICATION MLP NN

Image classification process has been applied on the PCA dataset containing 8 selected principal components and generally composed by 50 hours of ECG recording equally balanced into AF and NSR episodes. ECG records are related to 68 different patients and they have been stratified into 5 clusters containing approximatively 5 hours of AF records and 5 hours of NSR records each (Fig. 64).

Image classification has been achieved using several different feedforwards multilayer perceptron (MLP) neural network (NN) triangular configuration from 1 to 3 hidden layers. The number of neurons in the first hidden layer was ranged from 10 to 50 with steps of 10, and the number of neurons were halved for each addition hidden layer to obtain triangular configurations with fixed proportionality dimensions.

Each MLP NN architecture configuration has been trained with a balanced training set composed by 4 clusters of patients containing the same number of elements between the two class that approximately are 20 hours AF records and 20 hours NSR records. NNs have been tested with the remaining cluster of patients that has been used as testing set. Each NN architecture has been trained and tested 5 time for statistical validation since NN weight initialization is random.

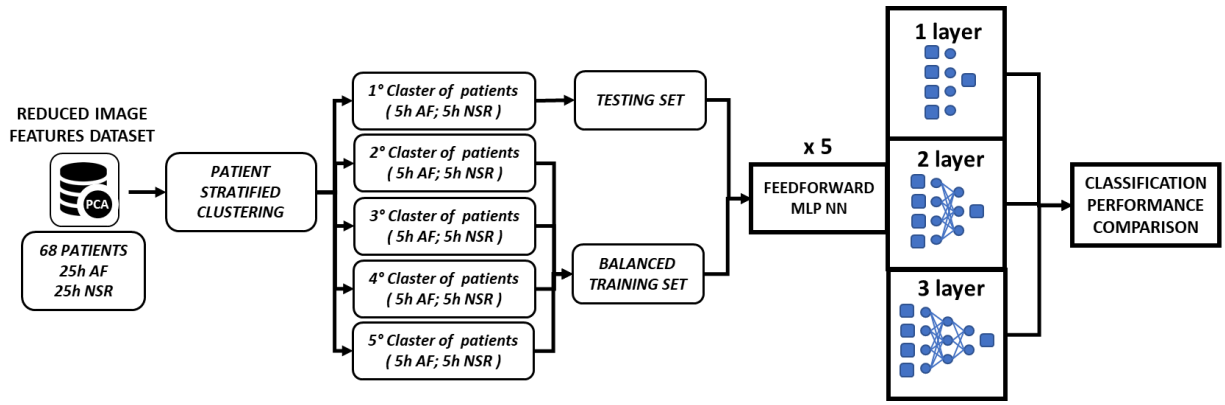

Figure 64

Classification performances of each NN architecture are shown in Fig 65. It is evident that best results (lower variability, higher accuracy) occurs with NN of 2 hidden layer containing 30-15 neurons respectively.

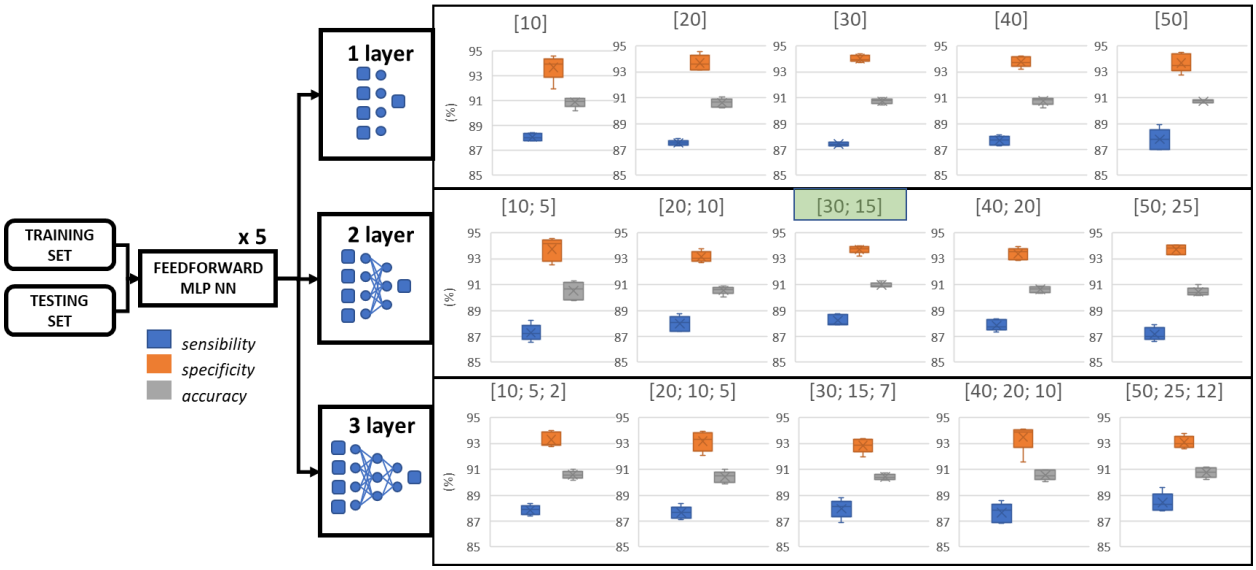

Figure 65

The selected NN configuration (2 hidden layer of 30-15 neurons) has been validated with 5 fold cross validation technique where iteratively each patient cluster has been used as testing set and remaining clusters used as training set (Fig. 66). At the end of k fold cross validation, all images have been classified and the results shown.

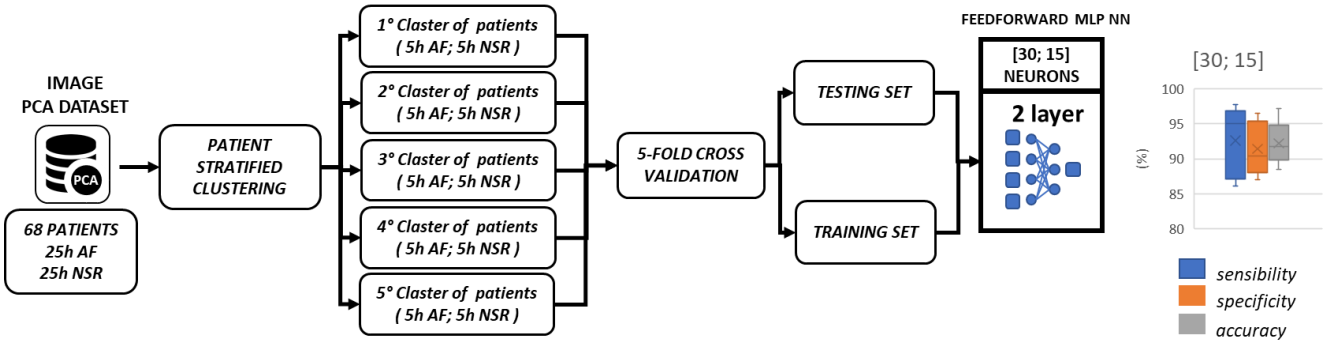

Figure 66

7 CONCLUSION

The AF detection algorithm was developed to be used in combination with ECG-WATCH device that records 10 seconds single lead ECG signal.

VITAL-ECG AF detection performances have been compared to other three single lead ECG portable device for AF diagnosis currently present on the market: KARDIA BAND, ImPulse, myDiagnostick.

KARDIA BAND (Fig.67) is a device produced by AliveCor company and ImPulse (Fig. 68) is a device produced by Plessey society. They both record 30 seconds single lead ECG signal. MyDiagnotick (Fig. 69) is a device produced by ABS company and it records ECG signals 30 to 60 seconds long.

Figure 67

Figure 68

Figure 69

ECG-WATCH device can achieve AF diagnosis with only 10 seconds ECG signal and its AF detection performance are comparable to performances of other devices (Fig 70):

- ECG-WATCH (10 sec): sensibility: 92,62%, specificity 91,44%, accuracy 92,21%
- KARDIA BAND (30 sec): sensibility: 93%, specificity 84%, accuracy 77%
- ImPulse (30 sec): sensibility: 96.14%, specificity 95.73%, accuracy 95.97%
- myDiagnostick (1 min): sensibility: 94%, specificity 93%, accuracy 93,5%

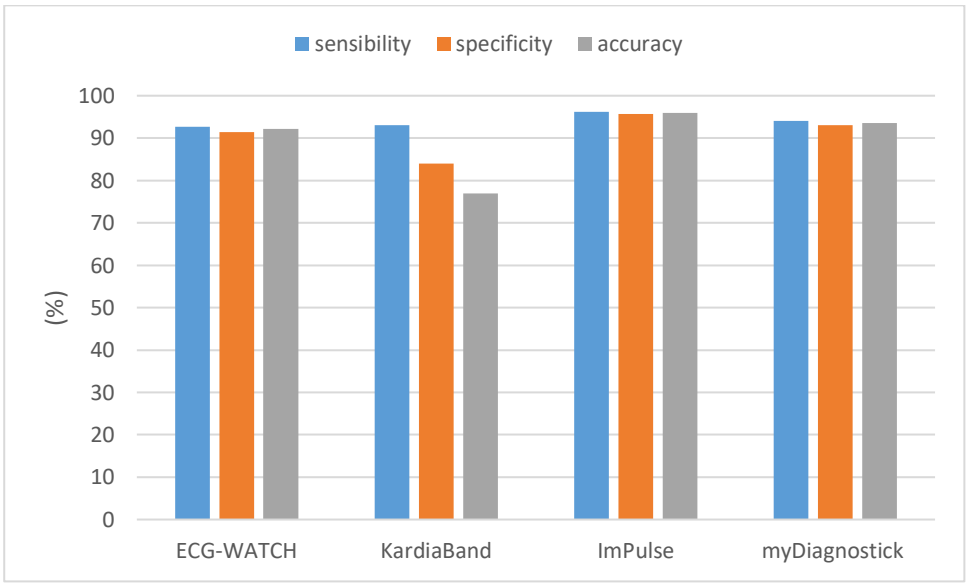

Figure 7067

8 APPENDIX A

WAVELET BASED DETECTOR

id	fp	fn	vp	ann	accuracy	sensitivity	F1_score	precision
100	0	0	2272	2272	100	100	100	100
101	4	0	1864	1864	99,78	100	99,89	99,78
102	1	0	2186	2186	99,95	100	99,97	99,95
103	1	0	2083	2083	99,95	100	99,97	99,95
104	27	0	2228	2228	98,8	100	99,39	98,8
105	36	6	2565	2571	98,38	99,76	99,18	98,61
106	1	0	2026	2026	99,95	100	99,97	99,95
107	1	1	2135	2136	99,9	99,95	99,95	99,95
108	52	6	1756	1762	96,8	99,65	98,37	97,12
109	0	0	2531	2531	100	100	100	100
111	2	1	2122	2123	99,85	99,95	99,92	99,9
112	1	0	2538	2538	99,96	100	99,98	99,96
113	0	0	1794	1794	100	100	100	100
114	5	0	1878	1878	99,73	100	99,86	99,73
115	0	0	1952	1952	100	100	100	100
116	2	17	2394	2411	99,21	99,29	99,6	99,91
117	0	0	1534	1534	100	100	100	100
118	1	0	2277	2277	99,95	100	99,97	99,95
119	3	0	1986	1986	99,84	100	99,92	99,84
121	1	1	1861	1862	99,89	99,94	99,94	99,94
122	1	0	2475	2475	99,95	100	99,97	99,95
123	0	0	1518	1518	100	100	100	100
124	1	0	1618	1618	99,93	100	99,96	99,93
200	9	0	2600	2600	99,65	100	99,82	99,65
201	7	1	1961	1962	99,59	99,94	99,79	99,64
202	4	2	2133	2135	99,71	99,9	99,85	99,81
203	21	19	2960	2979	98,66	99,36	99,32	99,29
205	1	4	2651	2655	99,81	99,84	99,9	99,96
207	13	134	2197	2331	93,72	94,25	96,76	99,41
208	4	14	2940	2954	99,39	99,52	99,69	99,86
209	2	0	3004	3004	99,93	100	99,96	99,93
210	4	16	2633	2649	99,24	99,39	99,62	99,84
212	0	0	2747	2747	100	100	100	100
213	0	2	3248	3250	99,93	99,93	99,96	100
214	3	1	2260	2261	99,82	99,95	99,91	99,86
215	2	0	3362	3362	99,94	100	99,97	99,94
217	3	0	2207	2207	99,86	100	99,93	99,86
219	1	0	2153	2153	99,95	100	99,97	99,95
220	0	1	2046	2047	99,95	99,95	99,97	100
221	1	3	2423	2426	99,83	99,87	99,91	99,95
222	3	0	2482	2482	99,87	100	99,93	99,87
223	1	0	2604	2604	99,96	100	99,98	99,96
228	43	1	2051	2052	97,89	99,95	98,93	97,94
230	3	0	2255	2255	99,86	100	99,93	99,86
231	1	0	1570	1570	99,93	100	99,96	99,93
232	18	0	1780	1780	98,99	100	99,49	98,99
233	0	2	3076	3078	99,93	99,93	99,96	100
234	1	0	2752	2752	99,96	100	99,98	99,96
total	285	232	109688	109920	99,53	99,78	99,76	99,74

9 APPENDIX B

PAN-TOMPKINS DETECTOR

id	fp	fn	vp	ann	accuracy	sensitivity	F1_score	precision
100	0	0	2272	2272	100	100	100	100
101	5	1	1863	1864	99,67	99,94	99,83	99,73
102	1	0	2186	2186	99,95	100	99,97	99,95
103	1	5	2078	2083	99,71	99,75	99,85	99,95
104	15	24	2204	2228	98,26	98,92	99,12	99,32
105	33	5	2566	2571	98,54	99,8	99,26	98,73
106	1	53	1973	2026	97,33	97,38	98,65	99,94
107	2	8	2128	2136	99,53	99,62	99,76	99,9
108	113	11	1751	1762	93,38	99,37	96,58	93,93
109	0	5	2526	2531	99,8	99,8	99,9	100
111	2	1	2122	2123	99,85	99,95	99,92	99,9
112	1	0	2538	2538	99,96	100	99,98	99,96
113	0	0	1794	1794	100	100	100	100
114	1	258	1620	1878	86,21	86,26	92,59	99,93
115	0	0	1952	1952	100	100	100	100
116	3	24	2387	2411	98,88	99	99,43	99,87
117	0	0	1534	1534	100	100	100	100
118	1	0	2277	2277	99,95	100	99,97	99,95
119	1	0	1986	1986	99,94	100	99,97	99,94
121	1	2	1860	1862	99,83	99,89	99,91	99,94
122	1	0	2475	2475	99,95	100	99,97	99,95
123	0	3	1515	1518	99,8	99,8	99,9	100
124	1	9	1609	1618	99,38	99,44	99,69	99,93
200	2	5	2595	2600	99,73	99,8	99,86	99,92
201	1	76	1886	1962	96,07	96,12	97,99	99,94
202	1	12	2123	2135	99,39	99,43	99,69	99,95
203	12	80	2899	2979	96,92	97,31	98,43	99,58
205	2	4	2651	2655	99,77	99,84	99,88	99,92
207	10	135	2196	2331	93,8	94,2	96,8	99,54
208	2	366	2588	2954	87,55	87,61	93,36	99,92
209	1	0	3004	3004	99,96	100	99,98	99,96
210	3	41	2608	2649	98,34	98,45	99,16	99,88
212	0	0	2747	2747	100	100	100	100
213	0	7	3243	3250	99,78	99,78	99,89	100
214	2	5	2256	2261	99,69	99,77	99,84	99,91
215	1	5	3357	3362	99,82	99,85	99,91	99,97
217	2	7	2200	2207	99,59	99,68	99,79	99,9
219	1	4	2149	2153	99,76	99,81	99,88	99,95
220	0	0	2047	2047	100	100	100	100
221	1	165	2261	2426	93,16	93,19	96,45	99,95
222	1	81	2401	2482	96,69	96,73	98,32	99,95
223	1	186	2418	2604	92,82	92,85	96,27	99,95
228	10	146	1906	2052	92,43	92,88	96,06	99,47
230	1	0	2255	2255	99,95	100	99,97	99,95
231	1	5	1565	1570	99,61	99,68	99,8	99,93
232	1	2	1778	1780	99,83	99,88	99,91	99,94
233	0	10	3068	3078	99,67	99,67	99,83	100
234	1	5	2747	2752	99,78	99,81	99,89	99,96
total	240	1756	108164	109920	98,18	98,4	99,08	99,77

BIBLIOGRAPHY

[1] Mairesse GH, Moran P, Van Gelder IC, et al. Screening for atrial fibrillation: a European Heart Rhythm Association (EHRA) consensus document endorsed by the Heart Rhythm Society (HRS), Asia Pacific Heart Rhythm Society (APHRS), and Sociedad Latinoamericana de Estimulación Cardíaca y Electrofisiología (SOLAECE) [published correction appears in Europace. 2018 Apr 1;20(4):658]. Europace. 2017;19(10):1589-1623. doi:10.1093/europace/eux177

[2] Duarte R, Stainthorpe A, Mahon J, et al. Lead-I ECG for detecting atrial fibrillation in patients attending primary care with an irregular pulse using single-time point testing: A systematic review and economic evaluation. PLoS One. 2019;14(12):e0226671. Published 2019 Dec 23. doi:10.1371/journal.pone.0226671

[3] Aswathy Velayudhan, Soniya Peter "Noise Analysis and Different Denoising Techniques of ECG Signal - A Survey" IOSR Journal of Electronics and Communication Engineering (IOSR-JECE), e-ISSN: 2278-2834, p- ISSN: 2278-8735. PP 40-44

[4] Rahul Kher (2019) Signal Processing Techniques for Removing Noise from ECG Signals. J Biomed Eng 1: 1-9.

[5] An X, K Stylios G. Comparison of Motion Artefact Reduction Methods and the Implementation of Adaptive Motion Artefact Reduction in Wearable Electrocardiogram Monitoring. *Sensors (Basel)*. 2020;20(5):1468. Published 2020 Mar 7. doi:10.3390/s20051468

[6] Aneja, Manpreet & Singh, Birmohan & Seema,. (2011). Comparison of different approaches for removal of Baseline wander from ECG signal. International Conference and Workshop on Emerging Trends in Technology 2011, ICWET 2011 - Conference Proceedings. 5. 1290-1294. 10.1145/1980022.1980307.

[7] Steven W. Smith. 1997. The scientist and engineer's guide to digital signal processing. California Technical Publishing, USA.

[8] Selcan Kaplan Berkaya, Alper Kursat Uysal, Efnan Sora Gunal, Semih Ergin, Serkan Gunal, M. Bilginer Gulmezoglu,"A survey on ECG analysis",Biomedical Signal Processing and Control,Volume 43,2018,Pages 216-235.

[9] Vest A, Da Poian G, Li Q, Liu C, Nemati S, Shah A, Clifford GD, "An Open Source Benchmarked Toolbox for Cardiovascular Waveform and Interval Analysis" Physiological Measurement (In Press) DOI:10.5281/zenodo.1243111; 2018.

[10] Goldberger AL, Amaral LAN, Glass L, Hausdorff JM, Ivanov PCh, Mark RG, Mietus JE, Moody GB, Peng CK, Stanley HE. "PhysioBank, PhysioToolkit, and PhysioNet: Components of a New Research Resource for Complex Physiologic Signals." Circulation 101(23):e215-e220 [http://circ.ahajournals.org/content/101/23/e215.full]; 2000 (June 13). PMID: 10851218; doi: 10.1161/01.CIR.101.23.e215

[11] Mabrouki, Rebeh & Khaddoumi, Balkine & Sayadi, Mounir. (2016). Atrial Fibrillation detection on electrocardiogram. 268-272. 10.1109/ATSIP.2016.7523112.

[12] Parks, Thomas W., and C. Sidney Burrus. Digital Filter Design. New York: John Wiley & Sons, 1987, pp. 54–83.

[13] Randazzo, Vincenzo & Ferretti, Jacopo & Pasero, Eros. (2019). ECG WATCH: a real time wireless wearable ECG. 1-6. 10.1109/MeMeA.2019.8802210.

[14] V. Randazzo, E. Pasero and S. Navaretti, "VITAL-ECG: A portable wearable hospital," *2018 IEEE Sensors Applications Symposium (SAS)*, Seoul, 2018, pp. 1-6, doi: 10.1109/SAS.2018.8336776.

[15] A. C. Mugdha, F. S. Rawnaque and M. U. Ahmed, "A study of recursive least squares (RLS) adaptive filter algorithm in noise removal from ECG signals," *2015 International Conference on Informatics, Electronics & Vision (ICIEV)*, Fukuoka, 2015, pp. 1-6, doi: 10.1109/ICIEV.2015.7333998.

[16]Poungponsri, Suranai & Yu, Xiao-Hua. (2013). An adaptive filtering approach for electrocardiogram (ECG) signal noise reduction using neural networks. Neurocomputing. 117. 206–213. 10.1016/j.neucom.2013.02.010.
[17]Thakor NV, Zhu YS. Applications of adaptive filtering to ECG analysis: noise cancellation and arrhythmia detection. *IEEE Trans Biomed Eng*. 1991;38(8):785-794. doi:10.1109/10.83591
[18]Martin Ester, Hans-Peter Kriegel, Jörg Sander, and Xiaowei Xu. 1996. A density-based algorithm for discovering clusters in large spatial databases with noise. In Proceedings of the Second International Conference on Knowledge Discovery and Data Mining (KDD'96). AAAI Press, 226–231.
[19]U. Satija, B. Ramkumar and M. S. Manikandan, "A New Automated Signal Quality-Aware ECG Beat Classification Method for Unsupervised ECG Diagnosis Environments," in IEEE Sensors Journal, vol. 19, no. 1, pp. 277-286, 1 Jan.1, 2019, doi: 10.1109/JSEN.2018.2877055.
[20]U. Satija, B. Ramkumar and M. S. Manikandan, "A Review of Signal Processing Techniques for Electrocardiogram Signal Quality Assessment," in IEEE Reviews in Biomedical Engineering, vol. 11, pp. 36-52, 2018, doi: 10.1109/RBME.2018.2810957.
[21]B. A. S. del Río, T. Lopetegi and I. Romero, "Assessment of different methods to estimate electrocardiogram signal quality," 2011 Computing in Cardiology, Hangzhou, 2011, pp. 609-612.
[22]U. Satija, B. Ramkumar and M. S. Manikandan, "Automated ECG Noise Detection and Classification System for Unsupervised Healthcare Monitoring," in IEEE Journal of Biomedical and Health Informatics, vol. 22, no. 3, pp. 722-732, May 2018, doi: 10.1109/JBHI.2017.2686436.
[23] H. Xia et al., "Computer algorithms for evaluating the quality of ECGs in real time," 2011 Computing in Cardiology, Hangzhou, 2011, pp. 369-372.
[24] D. Hayn, B. Jammerbund and G. Schreier, "ECG quality assessment for patient empowerment in mHealth applications," 2011 Computing in Cardiology, Hangzhou, 2011, pp. 353-356.
[25] X. Zhou, X. Zhu, K. Nakamura and N. Mahito, "ECG Quality Assessment Using 1D-Convolutional Neural Network," 2018 14th IEEE International Conference on Signal Processing (ICSP), Beijing, China, 2018, pp. 780-784, doi: 10.1109/ICSP.2018.8652479.
[26] Aboukhalil A, Nielsen L, Saeed M, Mark RG, Clifford GD. Reducing false alarm rates for critical arrhythmias using the arterial blood pressure waveform. J Biomed Inform. 2008 Jun;41(3) 442-451. doi:10.1016/j.jbi.2008.03.003. PMID: 18440873; PMCID: PMC2504518.
[27] C. Orphanidou, T. Bonnici, P. Charlton, D. Clifton, D. Vallance and L. Tarassenko, "Signal-Quality Indices for the Electrocardiogram and Photoplethysmogram: Derivation and Applications to Wireless Monitoring," in IEEE Journal of Biomedical and Health Informatics, vol. 19, no. 3, pp. 832-838, May 2015, doi: 10.1109/JBHI.2014.2338351.
[28] Köhler, Bert-Uwe & Hennig, C. & Orglmeister, Reinhold. (2003). QRS detection using zero crossing counts. Progress in Biomedical Research. 8. 138-145.
[29] RAI, HARI & Chatterjee, Kalyan. (2018). A unique Feature Extraction using MRDWT for Automatic Classification of Abnormal Heartbeat from ECG Big Data with Multilayered Probabilistic Neural Network Classifier. Applied Soft Computing. 10.1016/j.asoc.2018.04.005.
[30] Bezerra Marinho, Leandro & Nascimento, Navar & Souza, João & Gurgel, Mateus & Filho, Pedro Pedrosa & Albuquerque, V.H.C.. (2019). A novel electrocardiogram feature extraction approach for cardiac arrhythmia classification. Future Generation Computer Systems. 97. 10.1016/j.future.2019.03.025.
[31] Cuiwei Li, Chongxun Zheng and Changfeng Tai, "Detection of ECG characteristic points using wavelet transforms," in IEEE Transactions on Biomedical Engineering, vol. 42, no. 1, pp. 21-28, Jan. 1995, doi: 10.1109/10.362922.
[32] Sabut, Sukanta & Sahoo, Santanu & Kanungo, Bhupen & Behera, Suresh. (2017). Multiresolution wavelet transform based feature extraction and ECG classification to detect cardiac abnormalities. Measurement. accepted. 55-66. 10.1016/j.measurement.2017.05.022
[33] J. S. Sahambi, S. N. Tandon and R. K. P. Bhatt, "Using wavelet transforms for ECG characterization. An on-line digital signal processing system," in IEEE Engineering in Medicine and Biology Magazine, vol. 16, no. 1, pp. 77-83, Jan.-Feb. 1997, doi: 10.1109/51.566158.

[34]S. Kadambe, R. Murray and G. F. Boudreaux-Bartels, "Wavelet transform-based QRS complex detector," in IEEE Transactions on Biomedical Engineering, vol. 46, no. 7, pp. 838-848, July 1999, doi: 10.1109/10.771194.
[35]Singh, Brij & Tiwari, Arvind. (2006). Optimal selection of wavelet basis function applied to ECG signal denoising. Digital Signal Processing. 16. 275-287. 10.1016/j.dsp.2005.12.003.
[36]N. Das and M. Chakraborty, "Performance analysis of FIR and IIR filters for ECG signal denoising based on SNR," 2017 Third International Conference on Research in Computational Intelligence and Communication Networks (ICRCICN), Kolkata, 2017, pp. 90-97, doi: 10.1109/ICRCICN.2017.8234487.
[37]M. Vetterli, "Wavelets, approximation, and compression," in IEEE Signal Processing Magazine, vol. 18, no. 5, pp. 59-73, Sept. 2001, doi: 10.1109/79.952805.
[38]L. A. Kurgan and K. J. Cios, "CAIM discretization algorithm," in IEEE Transactions on Knowledge and Data Engineering, vol. 16, no. 2, pp. 145-153, Feb. 2004, doi: 10.1109/TKDE.2004.1269594.
[39]M. A. Akbar et al., "An Empirical Study for PCA- and LDA-Based Feature Reduction for Gas Identification," in IEEE Sensors Journal, vol. 16, no. 14, pp. 5734-5746, July15, 2016, doi: 10.1109/JSEN.2016.2565721.
[40]Chang, Yin-Wen & Lin, Chih-Jen. (2008). Feature ranking using linear SVM. Journal of Machine Learning Research - Proceedings Track. 3. 53-64.
[41]Quanquan Gu, Zhenhui Li, and Jiawei Han. 2011. Generalized Fisher score for feature selection. In Proceedings of the Twenty-Seventh Conference on Uncertainty in Artificial Intelligence (UAI'11). AUAI Press, Arlington, Virginia, USA, 266–273.
[42]M. Pechenizkiy, A. Tsymbal and S. Puuronen, "PCA-based feature transformation for classification: issues in medical diagnostics," Proceedings. 17th IEEE Symposium on Computer-Based Medical Systems, Bethesda, MD, USA, 2004, pp. 535-540, doi: 10.1109/CBMS.2004.1311770.
[43]Sarkar S, Ritscher D, Mehra R. A detector for a chronic implantable atrial tachyarrhythmia monitor. *IEEE Trans Biomed Eng*. 2008;55(3):1219-1224. doi:10.1109/TBME.2007.903707
[44]R. He et al., "Automatic Cardiac Arrhythmia Classification Using Combination of Deep Residual Network and Bidirectional LSTM," in IEEE Access, vol. 7, pp. 102119-102135, 2019, doi: 10.1109/ACCESS.2019.2931500.
[45] S. H. Jambukia, V. K. Dabhi and H. B. Prajapati, "Classification of ECG signals using machine learning techniques: A survey," 2015 International Conference on Advances in Computer Engineering and Applications, Ghaziabad, 2015, pp. 714-721, doi: 10.1109/ICACEA.2015.7164783.
[46] Shen, Chia-Ping & Kao, Wen-Chung & Yang, Yueh-Yiing & Hsu, Ming-Chai & Wu, Yuan-Ting & Lai, Feipei. (2012). Detection of cardiac arrhythmia in electrocardiograms using adaptive feature extraction and modified support vector machines. Expert Systems with Applications. 39. 7845–7852. 10.1016/j.eswa.2012.01.093.
[47] Jeen-Shing Wang, Wei-Chun Chiang, Yu-Liang Hsu, Ya-Ting C. Yang, ECG arrhythmia classification using a probabilistic neural network with a feature reduction method, Neurocomputing, Volume 116, 2013, Pages 38-45.
[48] İnan Güler, Elif Derya Übeylı˙, ECG beat classifier designed by combined neural network model,Pattern Recognition,Volume 38, Issue 2,2005,Pages 199-208.
[49] Maršánová, Lucie & Ronzhina, Marina & Smisek, Radovan & Vitek, Martin & Němcová, Andrea & Smital, Lukas & Nováková, Marie. (2017). ECG features and methods for automatic classification of ventricular premature and ischemic heartbeats: A comprehensive experimental study. Scientific Reports. 7. 10.1038/s41598-017-10942-6.
[50] Ji, Yinsheng & Zhang, Sen & Xiao, Wendong. (2019). Electrocardiogram Classification Based on Faster Regions with Convolutional Neural Network. Sensors. 19. 2558. 10.3390/s19112558
[51] Acharya, U Rajendra & Kumar, A & Lim, Choo & Iyengar, Sundararaj & Kannathal, N & Krishnan, S. (2004). Classification of Cardiac Abnormalities Using Heart Rate Signals: A Comparative Study. Medical & Biological Engineering & Computing. 42. 288-93. 10.1007/BF02344702.

[52] F. Andreotti, O. Carr, M. A. F. Pimentel, A. Mahdi and M. De Vos, "Comparing feature-based classifiers and convolutional neural networks to detect arrhythmia from short segments of ECG," 2017 Computing in Cardiology (CinC), Rennes, 2017, pp. 1-4, doi: 10.22489/CinC.2017.360-239.
[53] B. Mohammadzadeh-Asl and S. K. Setarehdan, "Neural network based arrhythmia classification using Heart Rate Variability signal," 2006 14th European Signal Processing Conference, Florence, 2006, pp. 1-4.
[54] R. Firoozabadi, R. E. Gregg and S. Babaeizadeh, "P-wave Analysis in Atrial Fibrillation Detection Using a Neural Network Clustering Algorithm," 2018 Computing in Cardiology Conference (CinC), Maastricht, Netherlands, 2018, pp. 1-4, doi: 10.22489/CinC.2018.087.
[55] O. Aligholipour, M. Kuntalp and S. Sadaghiyanfam, "Silent Paroxysmal Atrial Fibrillation Detection by Neural Networks Based on ECG Records," 2019 Scientific Meeting on Electrical-Electronics & Biomedical Engineering and Computer Science (EBBT), Istanbul, Turkey, 2019, pp. 1-4, doi: 10.1109/EBBT.2019.8741771.
[56] Bumgarner JM, Lambert CT, Hussein AA, et al. Smartwatch Algorithm for Automated Detection of Atrial Fibrillation. *J Am Coll Cardiol*. 2018;71(21):2381-2388. doi:10.1016/j.jacc.2018.03.003
[57] Y. Xia, N. Wulan, K. Wang and H. Zhang, "Atrial fibrillation detection using stationary wavelet transform and deep learning," 2017 Computing in Cardiology (CinC), Rennes, 2017, pp. 1-4, doi: 10.22489/CinC.2017.210-084.
[58] Martis, Roshan & Acharya, U Rajendra & Prasad, Hari & Chua, Kuang & Lim, Choo. (2013). Automated detection of atrial fibrillation using Bayesian paradigm. Knowledge-Based Systems. 54. 269–275. 10.1016/j.knosys.2013.09.016.
[59] Faust, Oliver & Shenfield, Alex & Kareem, Murtadha & Tan, Ru San & Fujita, Hamido & Acharya, U Rajendra. (2018). Automated detection of atrial fibrillation using long short-term memory network with RR interval signals. Computers in Biology and Medicine. 102. 10.1016/j.compbiomed.2018.07.001.
[60] Cui, Xingran & Chang, Emily & Yang, Wen-Hung & Jiang, Bernard & Yang, Albert C & Peng, Chung-Kang. (2017). Automated Detection of Paroxysmal Atrial Fibrillation Using an Information-Based Similarity Approach. Entropy. 19. 677. 10.3390/e19120677.
[61] He R, Wang K, Zhao N, et al. Automatic Detection of Atrial Fibrillation Based on Continuous Wavelet Transform and 2D Convolutional Neural Networks. *Front Physiol*. 2018;9:1206. Published 2018 Aug 30. doi:10.3389/fphys.2018.01206
[62] H. Kim, U. Erdenebayar, C. Kang, D. Kang and K. Lee, "Estimation of atrial fibrillation using arbitrary normal ECG segments based on convolutional neural networks," 2018 International Conference on Electronics, Information, and Communication (ICEIC), Honolulu, HI, 2018, pp. 1-2, doi: 10.23919/ELINFOCOM.2018.8330629.
[63] Park, Jinho & Lee, Sangwook & Jeon, Moongu. (2009). Atrial fibrillation detection by heart rate variability in Poincare plot. Biomedical engineering online. 8. 38. 10.1186/1475-925X-8-38.
[64] G. Tuboly, G. Kozmann, O. Kiss and B. Merkely, "Atrial Fibrillation Detection Based on Poincaré Plot and P Wave Analysis," 2019 12th International Conference on Measurement, Smolenice, Slovakia, 2019, pp. 17-20, doi: 10.23919/MEASUREMENT47340.2019.8779967.
[65] Y. Liu et al., "Diagnosis of AF based on time and frequency features by using a hierarchical classifier," 2017 Computing in Cardiology (CinC), Rennes, 2017, pp. 1-4, doi: 10.22489/CinC.2017.180-102.
[66] N. Larburu, T. Lopetegi and I. Romero, "Comparative study of algorithms for Atrial Fibrillation detection," 2011 Computing in Cardiology, Hangzhou, 2011, pp. 265-268.

[67] Hagiwara, Yuki & Fujita, Hamido & Oh, Shu Lih & Tan, Jen Hong & Tan, Ru San & Ciaccio, Edward & Acharya, U Rajendra. (2018). Computer-Aided Diagnosis of Atrial Fibrillation based on ECG Signals: A Review. Information Sciences. 467. 10.1016/j.ins.2018.07.063.
[68] Faust, Oliver & Hagiwara, Yuki & Tan, Jen Hong & Oh, Shu Lih & Acharya, U Rajendra. (2018). Deep learning for healthcare applications based on physiological signals: A review. Computer Methods and Programs in Biomedicine. 161. 10.1016/j.cmpb.2018.04.005.
[69] Alcaraz, Raúl & Rieta, José. (2010). A review on sample entropy applications for the non-invasive analysis of atrial fibrillation electrocardiograms. Biomedical Signal Processing and Control. 5. 1-14. 10.1016/j.bspc.2009.11.001.
[70] Park J, Lee S, Jeon M. Atrial fibrillation detection by heart rate variability in Poincare plot. *Biomed Eng Online*. 2009;8:38. Published 2009 Dec 11. doi:10.1186/1475-925X-8-38
[71] R. Mabrouki, B. Khaddoumi and M. Sayadi, "Atrial Fibrillation detection on electrocardiogram," 2016 2nd International Conference on Advanced Technologies for Signal and Image Processing (ATSIP), Monastir, 2016, pp. 268-272, doi: 10.1109/ATSIP.2016.7523112.
[72] S. Islam, N. Ammour and N. Alajlan, "Atrial fibrillation detection with multiparametric RR interval feature and machine learning technique," 2017 International Conference on Informatics, Health & Technology (ICIHT), Riyadh, 2017, pp. 1-5, doi: 10.1109/ICIHT.2017.7899003.
[73] Ruan, Xiuhua & Liu, Changchun & Liu, Chengyu & Wang, Xinpei & Li, Peng. (2011). Automatic detection of atrial fibrillation using R-R interval signal. Proceedings - 2011 4th International Conference on Biomedical Engineering and Informatics, BMEI 2011. 2. 644-647. 10.1109/BMEI.2011.6098492.
[74] S. Hargittai, "Is it possible to detect atrial fibrillation by simply using RR intervals?," Computing in Cardiology 2014, Cambridge, MA, 2014, pp. 897-900.
[75] M. Boshkovska, M. Gusev and V. Zdraveski, "Parallel Implementation of an Algorithm for Atrial Fibrillation Detection Using RR Intervals and Shannon Entropy," 2018 26th Telecommunications Forum (TELFOR), Belgrade, 2018, pp. 1-4, doi: 10.1109/TELFOR.2018.8612044.
[76] Goldberger AL, Amaral LAN, Glass L, Hausdorff JM, Ivanov PCh, Mark RG, Mietus JE, Moody GB, Peng C-K, Stanley HE. PhysioBank, PhysioToolkit, and PhysioNet: Components of a New Research Resource for Complex Physiologic Signals. Circulation 101(23):e215-e220 [Circulation Electronic Pages; http://circ.ahajournals.org/content/101/23/e215.full]; 2000 (June 13).
[77] G. D. Clifford et al., "AF classification from a short single lead ECG recording: The PhysioNet/computing in cardiology challenge 2017," 2017 Computing in Cardiology (CinC), Rennes, 2017, pp. 1-4, doi: 10.22489/CinC.2017.065-469.